LITHOS

Geochemistry and geochronology of the Corno Alto complex (Adamello batholith): insights on the early melts produced during Neo-Tethys subduction

--Manuscript Draft--

Manuscript Number:	LITHOS11565
Article Type:	Regular Article
Keywords:	Corno Alto; Alpine orogen; Adamello batholith; High Ba-Sr granitoids

Abstract:

The Corno Alto complex represents the onset of the intrusive igneous activity during the Alpine Orogen and for this reason has particular importance in the interpretation of the geodynamic evolution of the Alps. Three distinct types of granitoid rocks, ranging in composition from tonalite to granodiorite, characterize the Corno Alto complex. Whole-rock chemistry reveals peculiar features with respect to the other units of the Adamello batholith, and to typical I-type and S-type granitoid rocks. The Corno Alto rocks exhibit the highest SiO2 contents, K2O+Na2O up to 7.2%, a strong enrichment in Ba and to a minor extent in Sr (Ba + Sr ≈ 1100-1900 ppm). Other geochemical features include a moderately-to-strong enrichment in LREE over HREE (LaN/YbN > 20) and Y (Sr/Y > 40).

U-Pb geochronology on zircon on the whole intrusive complex suggests an incremental assembly of the Corno Alto complex by multiple and possibly discrete magma injections in a time span of about 5 My. The igneous activity shows an east-west decreasing age trend, with three main recurring age peaks, at ca. 44 Ma, ca. 42 Ma, and ca. 39 Ma. The different zircon domains have significantly distinct Hf isotopes (up to 18 ƐHf units of variation) with some values trending towards the isotopic composition of the depleted mantle (DM).

Major, trace element geochemistry and Hf isotope composition of zircon allow to distinguish at least two geochemically distinct components in the Corno Alto rocks: i) a high Ba component characterised by high Sr and La/Yb ratios, likely derived from melting of carbonate sediments of slab origin; ii) a juvenile component with Hf isotopic signature close to the depleted mantle and capable to crystallize plagioclase with An90 which is interpreted as the primitive mantle signal.

The occurrence of a carbonate input in the mantle derived melts implies that at 44 Ma thermal conditions were anomalous and high enough to allow carbonate melting in the subducting slab. These high thermal conditions parallel those at the Archean-Proterozoic transition and the Corno Alto complex could thus represent a kind of modern analogues of the high Ba/K sanukitoids.

Title page

Geochemistry and geochronology of the Corno Alto complex (Adamello batholith): insights on the early melts produced during Neo-Tethys subduction

Mosconi A.[a,*], Cannaò E.[a], Farina F.[a], Malusà M.G.[b], Zanchetta S.[b], Tiepolo M.[a]

[a] Department of Earth Sciences "A. Desio", Università degli Studi di Milano, Via Botticelli 23, 21133 Milan, Italy

[b] Department of Earth and Environment Sciences, University of Milano-Bicocca, Piazza della Scienza 4, 1-20126 Milan, Italy

*Corresponding author: **angelica.mosconi@unimi.it**

E-mail addresses: enrico.cannao@unimi.it (Cannaò E.); federico.farina@unimi.it (Farina F.); marco.malusa@unimib.it (Malusà M.G.); stefano.zanchetta@unimib.it (Zanchetta S.); massimo.tiepolo@unimi.it (Tiepolo M.)

Abstract

The Corno Alto complex represents the onset of the intrusive igneous activity during the Alpine Orogen and for this reason has particular importance in the interpretation of the geodynamic evolution of the Alps. Three distinct types of granitoid rocks, ranging in composition from tonalite to granodiorite, characterize the Corno Alto complex. Whole-rock chemistry reveals peculiar features with respect to the other units of the Adamello batholith, and to typical I-type and S-type granitoid rocks. The Corno Alto rocks exhibit the highest SiO_2 contents, K_2O+Na_2O up to 7.2%, a strong enrichment in Ba and to a minor extent in Sr (Ba + Sr ≈ 1100-1900 ppm). Other geochemical features include a moderately-to-strong enrichment in LREE over HREE (La_N/Yb_N > 20) and Y (Sr/Y > 40).

U-Pb geochronology on zircon on the whole intrusive complex suggests an incremental assembly of the Corno Alto complex by multiple and possibly discrete magma injections in a time span of about 5 My. The igneous activity shows an east-west decreasing age trend, with three main recurring age peaks, at ca. 44 Ma, ca. 42 Ma, and ca. 39 Ma. The different zircon domains have significantly distinct Hf isotopes (up to 18 ε_{Hf} units of variation) with some values trending towards the isotopic composition of the depleted mantle (DM).

Major, trace element geochemistry and Hf isotope composition of zircon allow to distinguish at least two geochemically distinct components in the Corno Alto rocks: i) a high Ba component characterised by high Sr and La/Yb ratios, likely derived from melting of carbonate sediments of slab origin; ii) a juvenile component with Hf isotopic signature close to the depleted mantle and capable to crystallize plagioclase with An_{90} which is interpreted as the primitive mantle signal.

The occurrence of a carbonate input in the mantle derived melts implies that at 44 Ma thermal conditions were anomalous and high enough to allow carbonate melting in the subducting slab. These high thermal conditions parallel those at the Archean-Proterozoic transition and the Corno Alto complex could thus represent a kind of modern analogues of the high Ba/K sanukitoids.

Keywords: Corno Alto, Alpine orogen, Adamello batholith, High Ba-Sr granitoids

Highlights

- The Corno Alto complex consists of three types of granitoid rocks
- The Corno Alto complex is chemically peculiar in the Adamello framework
- High Ba content likely derived from melting of carbonate sediments of slab origin
- The Corno Alto complex is a modern analogue of the high Ba/K sanukitoids

1. Introduction

The nature and composition of granitoid rocks significantly changed throughout the Earth's history highlighting major changes in the mechanisms of continental crust formation and differentiation (Laurent et al., 2014). The early continental crust is typically dominated by the tonalite-trondhjemite-granodiorite association, known as TTG (Hawkesworth et al., 2020), whose origin is ascribed to the partial melting of mafic lithologies either as subducting hydrated basalts (Foley et al., 2002) or in a overthickened eclogitic crust (Rapp et al., 2003). Many Archean cratons show the occurrence of younger intrusive intermediate-felsic rocks with different composition relative to TTG. These rocks, which are known as archean sanukitoids (Shirey and Hanson, 1984), are enriched in LILE (e.g. Sr, Ba and LREE) and exhibit a moderately high concentration in compatible elements (e.g. Mg, Ni, and Cr). Sanukitoids are interpreted to mark the change in the site of partial melting from the subducting slab to the mantle wedge (Fowler and Rollinson, 2012) as a consequence of a modified tectono-thermal regime. The progressive cooling of the Earth definitely marked the decline of both TTG and sanukitoids leaving the scene to Phanerozoic granitoid rocks. However, occasionally, compositional equivalents of sanukitoids, known as "high Ba-Sr" granites, are recognized and widespread in late Cretaceous and late Cenozoic orogenic belts (Fowler et al., 2008). Modern analogues of Archean-Proterozoic granitoids are extremely important because they may help recognizing not only occasional recurrences of thermal regimes similar to those in the Archean but also similar tectono-magmatic events.

The Corno Alto complex, the oldest intrusion in the Tertiary Adamello batholith (Schaltegger et al., 2019) resembles a TTG association (Lustrino et al., 2011). Being the oldest intrusion formed during the Alpine orogenesis (Ji et al., 2019), the Corno Alto complex is crucial to shed light into the tectono-magmatic conditions active at the onset of the Alpine magmatism; conditions that are not yet fully understood. Different models were proposed to account for magma generation during the Alpine Orogen such as post-collision lithospheric extension (Laubscher, 2010), slab-breakoff process (Blanckenburg and Davies, 1995) or progressive steepening of a continuous slab (e.g. Ji et al., 2019). In this frame, Ji et al. (2019) also suggested that, at the transition between the Alpine and Dinaric subductions, slab tear may have contributed to the genesis of adakite-like melts such as those reported in the Re di Castello Unit (Tiepolo and Tribuzio, 2005).

Despite the key importance in understanding the tectono-magmatic conditions at the onset of the Alpine Orogeny, a detailed geochemical and geochronological characterisation of the Corno Alto intrusive complex is still missing. This study aims to investigate the petrogenetic processes generating the early melts in the Alpine orogeny and their bearing on the general architecture of the Alpine evolution. We present a new comprehensive dataset combining whole-rock and in situ zircon geochemistry and geochronology (U-Pb dates, trace element compositions and Hf isotopes) on different lithotypes of the Corno Alto complex. Geochemical data revealed a high Ba-Sr character of the complex, peculiar compared to the other Adamello units, which is discussed in the light of recent geodynamic constraints for the Alpine region.

2. Geological setting

The Adamello batholith is the largest and oldest intrusion in the Alpine belt emplaced along the Periadriatic fault system during the Eocene and the early Oligocene, after the subduction of the Neo-Thetys ocean and the subsequent collision between the paleo-European and paleo-African continental plates (e.g., Callegari and Brack, 2002; Fig. 1a-b). The Adamello batholith consists of discrete petrographically and isotopically distinctive plutons (Ulmer et al., 1983) of calc-alkaline affinity ranging in composition from quartz-diorite to granodiorite (Dupuy et al., 1982). Mafic rocks are locally associated with coeval felsic lithologies, both as satellite bodies at the pluton margins and as syn-plutonic intrusions (Blundy and Shimizu, 1991). Based on whole-rock radiogenic isotope data, the Adamello batholith is interpreted as evolved by assimilation and fractional crystallization from a picrobasaltic parental magma (Ulmer et al., 1983; Kagami et al., 1991). This model has been recently confirmed by in situ Hf isotopes analyses in zircons from the different units of the batholith (Ji et al., 2019; Schaltegger et al., 2019).

The Corno Alto intrusive complex crops out in the eastern part of the batholith, close to the South Giudicarie Fault and includes the Sostino apophysis to the southeast (Fig. 1c-d). According to the literature the complex is granodioritic to trondhjemitic in composition (Schaltegger et al., 2019) and intruded into a low-grade Variscan basement (Rendena Schists). Recent geochronological U-Pb data on zircons (e.g., Ji et al., 2019; Schaltegger et al., 2019) identified the Corno Alto intrusion as the oldest magmatic unit of the

Adamello batholith with an average age of 43.47 ± 0.16 Ma. According to Relvini et al. (2022), the Corno Alto felsic rocks were formed by mixing between anatectic melts, generated in the lower crust, and melts produced by fractional crystallization of mantle-derived magmas.

3. Methods

Whole rock major and trace element analyses were carried out at the Central Analytical Facility (CAF) of the Stellenbosch University, South Africa. Major element compositions were determined by X-ray fluorescence on fused discs with a PANalytical Axios Wavelenght Dispersive spectrometer equipped with a Rh tube at 3kW operating power. The standards used in the calibration procedures for major element analyses were BE-N and BHVO-1 (basalts), JB-1 (depleted-basalt), and JG-1 (granodiorite). Accuracy is better than 1% for major elements present at a concentration of greater than 1 wt% (Table A.1).

Bulk trace element concentrations were determined on the same materials by LA-ICP-MS using an Agilent 8800 ICP-MS coupled with a 193 nm M50 excimer laser normalizing to NIST SRM 612 glass (Jochum et al., 2011). Data reported in this study represent the average of four ablation spots. Certified BCR and BHVO basaltic glass (GeoReM database), BHVO and BCR powder (Jochum et al., 2016) were used as reference material. Data reduction was carried out using Iolite v. 3.71 software. Analytical accuracy is typically better than 12% (Table A.2).

Major element compositions of rock-forming minerals (plagioclase, epidote, biotite and white-mica) were measured at the Department of Earth Sciences "A. Desio" (ESD), University of Milano (Italy) by electron microprobe JEOL Superprobe 8200. The analyses were performed with a WDS system at 15.0 kV, 5nA for the electron beam and 1 μm beam size. Natural minerals were used as standards for the different elements (the numbers refer to the international standards): Mg on olivine 153, Fe on fayalite 143, Na on omphacite 154, Ti on ilmenite, Mn on rodonite, K on K-feldspar 113, Al and Ca on anorthite 137, Cr on metallic/pure Cr and Si on wollastonite.

Samples selected for zircon separation were crushed and sieved to a grain size of ca. 250 μm. Zircon crystal separation process included hydrodynamic, magnetic (Frantz), and dense-liquid separation using diiodomethane. Zircon grains were mounted in epoxy resin, polished, and then characterized for internal structure and inclusions using a JEOL JSM-IT 500 scanning electron microscope (SEM) equipped with a Deben Centaurus cathodoluminescence (CL) detector at the ESD.

Zircon trace element composition and U-Pb dating were carried out by Laser-Ablation Inductively Coupled Plasma Mass Spectrometry (LA-ICP-MS) at the ESD using a Thermo Fisher Scientific iCAP RQ ICP-MS coupled to a 193nm Excimer Laser Ablation System (Analyte Excite by Teledyne Cetac Technologies). Conditions for trace element determinations in zircon were: spot diameter of 25 µm, repetition rate of 10 Hz and a fluence of 2 J/cm^2. Helium was used as carrier gas with flow rates of 0.500 l/min in the sample cell, and 0.200 l/min in the cup. The SiO_2 concentration in zircon was fixed at the stoichiometric value of 32.78% wt.% and used as internal standard. Glass reference materials NIST-SRM 612 (Jochum et al., 2011) and BCR-2G (GeoReM database) were used as external standard and as quality control, respectively. On the glass references the spot diameter was set at 40 µm, repetition rate at 10 Hz and fluence at 6 J/cm^2 (NISTSRM612) and 3 J/cm^2 (BCR-2G).

The same LA-ICP-MS instrumentation was used for U-Pb zircon geochronology. The analyses were carried out with a laser spot of 25 µm, a laser fluence of 3 J/cm^2, and a repetition rate of 7 Hz. Helium flow rate within the ablation cell were the same reported for trace element determinations. The reference materials 91500 zircon (Wiedenbeck et al., 2004) and Plešovice zircon (Sláma et al., 2008) were used as external standard and quality control, respectively. Data reduction was carried out with the Glitter software (Griffin et al., 2008) whereas concordia age calculation was performed with IsoplotR (Vermeesch, 2018).

In-situ Hf isotope analyses were carried out on the same zircon domains selected for U-Pb dating, using the same laser ablation system previously mentioned but connected with a Thermo Fisher Scientific MC-ICP-MS Neptune XT at ESD. The initial $^{176}Hf/^{177}Hf$ ratio and initial εHf was calculated for each spot analysis according to the corresponding U/Pb date. Analyses were carried out with a laser repetition rate of 6 Hz and a beam diameter of 50 µm. Laser fluence was set at 3.5 J/cm^2. Errors are reported as 2 standard error (2s). The detailed analytical procedure was similar to that described by Fisher et al. (2014) and is given in the Supplementary Materials. The determined

$^{175}Hf/^{177}Hf$ ratios of 0.282675 ± 0.000047 (2s; n=58) for Temora-2 and of 0.282486 ± 0.000044 (2s; n=60) for Plesovice standards are in good agreement with the reported values (Sláma et al., 2008; Woodhead and Hergt, 2005).

4. Sampling and petrography

Detailed samples location with GPS coordinates are reported in the Supplementary Table A.3. Four main lithologies were identified and sampled in the Corno Alto complex, including the Sostino apophysis (Fig. 1c-d, Table A.3). A two-mica granodiorite (TMG) is the dominant lithology in the central and western part of the complex and nine samples were selected. Occasionally a porphyritic tonalite (PTN) and an equigranular tonalite (ETN), are found in the central and north-eastern part of the unit, respectively. Four representative tonalite samples were considered. An epidote-bearing granodiorite (EBG) dominates in the Sostino apophysis and four samples were selected (Fig. 1d). Clear relationships between the different lithologies were not recognised in the field due to the extensive vegetation. Sampling included for comparison purposes also one sample from a km scale diorite body cropping out northwest to the Corno Alto pluton (MDR), and one sample of tonalites (OTN) from the Mt. Ospedale area.

4.1 Two-mica granodiorites (TMG)

Two-mica granodiorites are fine- to medium-grained and contain 35-45% plagioclase, 25-35% quartz, 10-15% biotite, 5-10% K-feldspar and 5% white mica. Accessory minerals are magnetite, titanite, apatite, and zircon. Plagioclase is subhedral to euhedral and occurs as: (i) individual crystals up to 1 cm in size, commonly displaying evidence of resorption (Fig. 2a); (ii) centimetric monomineralic *glomerocrysts* (Hogan, 1993) consisting of several subhedral to anhedral plagioclase crystals (Fig. 2b). Rarely, small crystals (< 400 µm) of epidote, often showing allanite inner domains, were found enclosed in some plagioclase cores (Fig. 2c). Biotite has euhedral to subhedral habitus and rarely exceeds 1 mm in size. It occurs mainly as interstitial grains between plagioclase, K-feldspar, and quartz but it may occur also as inclusions inside plagioclase and white mica (Fig. 2c). Primary white mica is generally millimetric in size, subhedral and with equilibrium contacts with plagioclase and biotite (Fig. 2d). Alkali-feldspars occur both as anhedral perthitic microcline crystals and as small interstitial grains. Quartz occurs either as tiny interstitial crystals in a fine assemblage along some grain boundaries or as large grains (up to 4 mm) forming nodules that give a pseudo-porphyric texture to the rocks.

4.2 Tonalites (ETN and PTN)

Based on rock-texture, two types of tonalites were found: (i) equigranular (ETN) and (ii) porphyric (PTN) tonalite. The ETN are generally medium-grained with crystal reaching up to 4 mm in size while in the PTN plagioclase crystals may exceed one centimetre in length. Both types consist of plagioclase (50-60%), quartz (25-35%), biotite (10-15%), and minor interstitial K-feldspar and igneous epidote. Accessory phases are magnetite, allanite, titanite, and zircon. In ETN, plagioclase is subhedral to euhedral and occurs either as small, partially resorbed crystals or as bigger crystals forming *glomerocrysts*. Differently, in PTN plagioclase occurs also as euhedral centimetric-size grains (Fig. 2e) characterized by oscillatory zoning and by an external rim enriched of tiny quartz inclusions (Fig. 2f). In both types, biotite is euhedral to subhedral and occasionally occurs as inclusion hosted within the rim of plagioclase large crystals. Quartz and K-feldspar are anhedral and interstitial. Weakly pleochroic epidote (< 500 µm in dimensions) with euhedral to subhedral shapes, occurs as minor phase (< 1 vol.%). The sharp contacts with biotite, the euhedral habit when included into biotite and its occurrence as overgrowth on euhedral allanite grains are evidence for its igneous origin (Fig. 2g-h).

4.3 Epidote-bearing granodiorites (EBG)

A fine- to medium-grained epidote-bearing granodiorite is the main lithology in the Sostino apophysis. Major phases are plagioclase (35-40%), quartz (25-35%), biotite (10-15%), K-feldspar (10%) and epidote (5%). Apatite, titanite, zircon, magnetite, and allanite are common accessory minerals with relatively large dimensions (up to 1mm). EBG rocks are texturally very similar to the two mica granodiorites of the Corno Alto, mainly for the occurrence of rounded quartz nodules and for the widespread occurrence of plagioclase *glomerocrysts*. However, the mineralogy of the Sostino granodiorite is more similar to that observed in the tonalites being characterized by the occurrence of abundant igneous epidote as a major mafic phase (Fig. 2i), and the absence of primary white mica.

4.4 Diorites (MDR)

Dioritic rocks (CA19-3) are medium to fine grained and mainly consist of hornblende (45 vol%), plagioclase (40 vol.%), biotite (10 vol.%), and quartz (5 vol.%). Accessory minerals are zircon, apatite, and oxides. Hornblende occurs in fine-grained aggregates of acicular crystals often in association with biotite crystals. Plagioclase (0.5-2.5 mm in size) has subhedral habit and often shows resorption rims. Biotite has subhedral to euhedral habit and occur both in association with hornblende and as inclusion in plagioclase crystals. Quartz shows anhedral habit.

4.5 Mt. Ospedale tonalites (OTN)

Tonalitic rocks from the Mt. Ospedale (sample CA19-8) are medium- to coarse-grained with porphyric texture. They consist of euhedral to subhedral amphibole (up to 1 cm across), biotite (<7 mm), and plagioclase (up to 3 mm) dispersed in a finer grained matrix of quartz, biotite, plagioclase and microcline. Mineral proportions are: plagioclase (45 vol.%), quartz (20 vol.%), biotite (17 vol.%), amphibole (13 vol.%), microcline (5 vol.%). Accessory minerals are apatites, zircons, titanites and oxides. The euhedral coarse plagioclase grains have complex zoning and polysynthetic twinning. Those in the groundmass are tiny, subhedral with local resorption in correspondence of the crystal's core. The groundmass plagioclase is commonly associated with anhedral quartz grains and tiny subhedral microcline crystals. Biotite often shows inclusions of plagioclase, apatite, and oxides. Amphibole euhedral coarse crystals are green in colour and show inclusions of partially chloritized biotite, apatite, oxide and plagioclase.

5. Whole-rock geochemistry

Whole-rock major and trace element compositions of the Corno Alto rock suite are reported in Table A.4. The Corno Alto and Sostino granitoid rocks are calcic, with only a few samples that straddle the boundary with the calc-alkaline field (Fig. 3a). The granitoids are both metaluminous and peraluminous (0.98 ≤A/CNK≥ 1.20; Fig. 3b), silica-rich and (65.3 ≤SiO_2≤ 71.5 wt.%, Fig. 3a) characterized by relatively low K_2O/Na_2O ratios (ranging from 0.35 to 0.80). According to the normative feldspar classification diagram for the granitoid rocks (An-Ab-Or, Barker, 1979), the Corno Alto and Sostino rocks plot on the granodiorite and tonalite fields (Fig. 3c) and follow a trondhjemitic trend in the ternary K-Na-Ca plot (Fig. 3d; e.g., Macera et al., 1983). Remarkably, although these rocks have been commonly referred to as "trondhjemites" in the literature (Macera et al., 1983; Relvini et al., 2022), none of the studied samples plot in the trondhjemite field. Diorite and the Mt. Ospedale tonalite are metaluminous (A/CNK≤ 1.0) and less evolved (49.4 ≤ SiO_2 ≤ 62.9 wt.%) than the Corno Alto lithologies but with similar K_2O/Na_2O ratios.

Major element compositions (normalized to 100 wt.% anhydrous) were plotted in Harker diagrams using SiO_2 content on the x-axis (Fig. 4). The TMG rocks have the highest SiO_2 content close to 70.0 wt% and Mg# (molar ratio Mg/(Mg+Fe)) ≈ 0.40. These samples also display the lowest CaO (2.39- 3.25 wt%), $Fe_2O_{3(tot)}$ (1.89-2.41 wt.%), MgO (0.62-0.84 wt.%), and TiO_2 (≈ 0.22 wt.%) contents. K_2O is quite variable, ranging from 1.58 to 3.14 wt.%. These rocks represent the most peraluminous rocks with A/CNK ≥ 1.10 (Fig. 3b). Compared to the TMG, the EBG rocks have slightly lower SiO_2 contents (≈ 69 wt.%), similar Na_2O, K_2O and $Fe_2O_{3(tot)}$, but slightly higher CaO (up to 3.51 wt.%), TiO_2 (≈ 0.32 wt.%) and MgO (0.89-1.05 wt.%) contents. They are also characterized by a slightly metaluminous character (0.98 ≤ A/CNK ≥ 1.03; Fig. 3b). Both ETN and PTN rocks are less evolved in compositions, with SiO_2 ≈ 66 wt.%, and higher CaO (4.13-4.46 wt.%), Al_2O_3 (up to 17.9 wt.%), $Fe_2O_{3(tot)}$ (up to 3.93 wt.%), MgO (1.37-1.66 wt.%), and TiO_2 (≈ 0.40 wt.%) than the granodiorites. K_2O abundances are comparable to those of the less potassic TMG, while Na_2O and MnO are in the range of all the other rocks. Mg# is ≈ 0.45, similarly to the EBG rocks. The dioritic rocks (MDR) have lower SiO_2 (49.3 wt.%) and higher Fe_2O_3 (9.38 wt.%), CaO (9.11 wt.%), TiO_2 (1.32 wt.%) and MgO (9.72 wt.%) at comparable Al_2O_3, K_2O and Na_2O with the more evolved lithotypes of the CA unit. The Mt. Ospedale tonalite is lower in SiO_2 (62.6 wt.%) and Na_2O contents (3.01 wt.%) compared to the CA tonalites. Whereas higher TiO_2 (0.62 wt.%), Fe_2O_3 (5.37 wt.%), CaO (5.52 wt.%), and MgO contents (2.22 wt.%) are observed.

The chondrite normalized REE patterns (see Fig. D.1 in the supplementary materials) of the studied rocks are all characterized by strong enrichment in LREEs (up to 500 times chondrites) over HREEs (< 10 times chondrites). The $(La/Yb)_N$ ratio range from 14.2 to 30.7 in both TMG and EBG whereas is up to 61.2 in both types of tonalitic rocks (ETN and PTN). Eu anomaly is not pronounced (Eu/Eu* ≈ 0.80-1.04). Diorites and the Mt. Ospedale tonalite (MDR and OTN) show less fractionated REE patterns ($[La/Yb]_N$: 13.1-14.2) and a more pronounced negative Eu anomaly (Eu/Eu* ≈ 0.76-0.93).

The primitive mantle normalized trace element pattern (Fig. 5a) is characterized by negative Nb, Ta, P, and Ti anomalies relative to the neighbouring elements and by enrichments in K, Pb, U, Th and LILEs (especially Sr and Ba; Fig. 5b). The highest Sr contents (884 ppm) pertain to the PTN tonalitic rocks whereas the epidote-bearing granodiorites (EBG) and the two-mica granodiorites (TMG) are characterized by slightly lower contents (404-551 ppm) but still higher than those characterizing the diorites (MDR), the Mt. Ospedale tonalites (OTN). The epidote-bearing granodiorites (EBG) are Ba-rich (1069-1614 ppm) and exhibit higher Pb, Th and U concentrations compared to the other rock types. The concentration in high-field strength elements (HFSE) is similar in the different rock types with the exception for the diorites (MDR) and Mt.Ospedale tonalites (OTN).

6. Mineral Chemistry

Representative compositions of the analysed minerals are given in Appendix B.

Plagioclase

The total range of plagioclase composition in the Corno Alto unit is An_{92-12}, with the majority of analysis ranging between An_{30} and An_{40} and minor differences between the different lithotypes (Table B.1). The EBG rocks display the most albitic compositions with less variation in An contents from the core (An_{35-37}) to the rim (An_{13-22}). Plagioclase crystals from the TMG glomerocrysts display andesine composition at the core (An_{30-50}) and mostly oligoclase composition at the rims (An_{14-35}). TMG rocks contain sporadic plagioclase cores with high-An contents (up to An_{87}). These crystals are normally zoned and are characterized by an abrupt decrease in An (An_{rim12}) at their external margin featuring. ETN rocks display the narrowest range of An contents (An_{30-69}). Plagioclase crystals in the PTN display discrete compositional variations: An_{45-65} at the cores and An_{25-40} at the rims. Moreover, in these rocks few plagioclase crystals with extremely Ca-rich cores (up to An_{92}) followed by more albitic composition at the rim (An_{23}) were found. Plagioclase from diorites show a narrow compositional variability (An_{42-56}). Plagioclase crystals from OTN rocks have compositions varying from An_{41} to An_{73}.

Biotite

Biotite (Table B.2) from TMG rocks have Fe# [$Fe^{2+}/(Fe^{2+} + Mg^{2+})$] ranging from 0.46 to 0.51 and TiO_2 contents are between 1.85 and 2.68 wt.%.

In ETN and PTN rocks, biotite has variable Fe# in the range 0.33-0.95 and TiO_2 spanning from 2.03 to 2.76 wt.%. In EBG rocks, biotite crystals have major element composition analogous with that of the crystals in the TMG rocks (Fe#: 0.46-0.49; TiO_2 ranging from 2.38 to 3.46 wt.%). MDR biotites exhibit Fe# ranging from 0.38 and 0.45 and TiO_2 from 2.13 to 2.49 wt.%. In OTN rocks, biotite shows Fe# of 0.50-0.51 and TiO_2 contents in the range 2.13-2.49 wt.%.

Epidote

Epidote shows narrow compositional variations in the different rock types (Table B.3). Pistacite content (Ps = molar [Fe^{3+}/(Fe^{3+} + Al)] x100) varies between 21.1 and 30.3 %, with most of the compositions with pistacite content > 26%, for both interstitial epidote and epidote inclusions into plagioclase. TiO_2 contents are below 0.2 wt.% for all analysed grains. The euhedral habit, the allanite-rich cores, the Ps content varying between 24 and 35 mol% and the low TiO_2 contents (<0.2) are all evidences supporting an igneous origin of the epidote (Schmidt and Poli, 2004).

White mica

White mica occurs exclusively in the TMG (Table B.4). Si contents are slightly higher than typical muscovites from peraluminous granitoids (3.09 - 3.18 a.p.f.u., based on 11 oxygen) and point to low-Si phengites compositions.

Amphibole

Amphibole in MDR and OTN is hornblende in composition (Table B.5). The Mg# [$Mg/(Mg+Fe^{tot})$, in apfu] of amphibole in MDR is slightly higher (0.57-0.61) than in OTN (0.47-0.52). TiO_2 is in the range 0.65-1.20 wt.% in MDR amphiboles whereas it does not exceed 0.9 wt.% in those from OTN. Alkali contents (Na+K) range from 0.45 to 0.55 in OTN, while in MDR values vary from 0.32 to 0.47.

7. U-Pb zircon geochronology

At least two samples for each of the main lithologies of the Corno Alto complex were selected for U-Pb zircon geochronology, trace element and in-situ Hf isotope determinations. U-Pb ages and U-Pb Concordia diagrams are presented in the supplementary materials (Table C.1, Fig. D2-3). Analyses yielding >2% discordancy were not considered.

Based on CL properties, three different recurring domains, variably combined, were identified in zircons from the Corno Alto lithologies (Fig.6). A-type domains are characterized by oscillatory zoning and medium- to low-luminescence. B-type domain are unzoned to weakly zoned, characterized by medium- to high-luminescence, often displaying a dissolution surface at their boundary. Finally, C-type domains have rounded boundaries and exhibit bright luminescence with no significant apparent zoning. We anticipate that the distinction between A- and B-type domains is not geochronologically feasible. Therefore, in presenting ages, exclusive reference will be made to C-type domains. The U-Pb weighted mean ages of magmatic zircon grains are reported in figure 7.

7.1 Two-mica granodiorites (TMG)

Zircons from the two-mica granodiorites are prismatic to stubby, ranging in size from 75 µm to 400 µm. The length/width ratio is typically 2.5:1 to 4:1. Most of zircon grains have C-type and B-type cores mantled by domains with A-type texture. Only a subset of grains shows only A-type domains.

In sample CA19-10, thirty-one analyses were carried out. Of these, nine analyses yield discordant dates and were discarded. Six analyses on inherited crystals (C-type textures) yielded dates ranging from 449 ± 9 Ma to 980 ± 20 Ma. The remaining twenty-four analyses on both cores and rims do not allow calculating a single mean concordia age. On a probability density plot the analyses reveal the occurrence of at least two distinct U-Pb age populations. Most of the analyses define a main age peak at 39.1 ± 0.3 Ma (MSWD for c+e: 1; Fig.7). A subset of A-type domains rimming C-type cores yield an older age peak at 43.4 ± 0.4 Ma (MSWD for c+e = 2.8).

Fourteen analyses were performed on zircon grains of sample CA19-13. Of these, two analyses yield discordant ages. Twelve analyses yield concordant dates that allowed to calculate a mean concordia age at 43.6 ± 0.4 Ma (n=12, MSWD for c+e = 1.4).

In sample CA19-37, twenty-five analyses were carried out. Of these, four analyses gave discordant dates whereas six analyses returned U-Pb ages ranging from 471 ± 12 Ma to 2461 ± 71 Ma. The remaining fifteen analyses suggest the occurrence of two zircon populations with distinct U-Pb ages: most of the analyses yield a mean concordant age of 41.7 ± 0.4 Ma (n=11; MSWD for c+e = 0.43), whereas few analyses gave an older mean concordant age at 44.4 ±0.7 Ma (n= 4; MSWD for c+e = 0.25).

Fifty-four analyses have been carried out on sample CA19-41. Eleven analyses returned discordant ages whereas fourteen analyses carried out on C-type domains gave old and highly variable ages, from 151 ± 7 Ma to 1068 ± 30 Ma. Most of the analyses yield a mean concordia age at 43.7 ± 0.3 Ma (n=21; MSWD for c+e = 1.3). A subset of eight analyses yielded younger mean concordia age at 41.4 ± 0.5 Ma (n=8; MSWD for c+e = 0.7).

7.2 Tonalites (ETN and PTN)

Zircons from tonalite rocks are mostly prismatic, rarely with stubby habitus. They range in dimensions from ~100 µm to more than 300 µm with a typical length/width ratio of 2.5:1.

In sample CA19-16, (PTN) most of the zircon crystals display A-type domains in correspondence of both core and rim. Few zircon cores display B-type and C-type textures surrounded by A-type textures. Sixty-four analyses were carried out on the zircon grains from PTN rock CA19-16. Of these, seven analyses were discordant. Five analyses on C-type domains returned dates spanning from 186 ± 4 Ma to 867 ± 19 Ma. Fifty analyses on both cores and rims revealed the occurrence of two populations with distinct U-Pb ages. Most of the analyses yield a mean concordant age at 41.9 ± 0.2 Ma (n= 37; MSWD for c+e = 0.79); another subset of fifteen analyses returned older concordant dates and a mean concordia age at 44.2 ± 0.3 Ma (n=14; MSWD for c+e = 0.75).

Most of zircon crystals in sample CA19-21 (ETN) have A-type textures and only one core with C-type texture was found. Thirty-eight spot analyses in zircon grains from CA19-21 were performed. Of these, fifteen analyses are discordant. Twenty-three analyses yield a mean concordia age at 44.7 ± 0.3 Ma (n=23; MSWD for c+e = 0.7). One analysis performed on a C-type domain returned an age of 433 Ma ± 11 Ma.

7.3 Epidote-bearing granodiorites (EBG)

Most zircons from epidote- bearing granodiorites are prismatic, with elongated shape, sharp facets, and pointed tips. Zircon crystals are mainly colourless and transparent, with lengths ranging from 50 to 300 µm and length/width ratio of 2.5:1.

In sample CA19-26, zircon grains have either A-type and C-type cores. Forty-one analyses were carried out and of these, three analyses were discordant and ten analyses on C-type domains gave dates from 333 ± 18 Ma to 2174 ± 64 Ma. Twenty-eight analyses were concordant and yielded a mean concordia age at 44.0 ± 0.3 Ma (n=28; MSWD for c+e = 0.43).

In sample CA19-30, all grains display cores and rims with A-type texture while no B- or C-type domains were found. Twenty-seven analyses were carried out and twenty-two analyses of both cores and rims yield concordant dates and returned a mean concordia age at = 44.3 ± 0.3 Ma (n=22, MSWD for c+e = 0.52).

7.4 Diorite (MDR)

Zircon grains from the diorite (CA19-3) are mostly fractured with fragments reaching 300 µm in size. Zircon CL textures are peculiar and cannot be classified into A- B- or C-type domains. Zircons are characterised by patchy textures with faint zoning and irregular longitudinal streak as well as occasional spongy textures at the core. Seventeen analyses were performed on zircon grains from sample CA19-3. Of these, one returned discordant date. Fifteen analyses yield a mean concordant age at 39.7 ± 0.4 Ma (MSWD for c+e = 0.56). One analyses on a zircon core gave a date at 44.8 ± 1.4 Ma.

7.5 Mt. Ospedale tonalite (OTN)

Zircons from the Mt. Ospedale tonalite (CA19-8) are prismatic to stubby, ranging in dimension from to 300 µm, with length/width ratio of 2.5:1 to 4:1.

Most of zircon grains are characterised by cores and rims with A-type texture. Twenty-two analyses were carried out and two analyses on C-type domains returned dates at 736 ± 36 Ma and 941 ± 54 Ma. The remaining twenty analyses on both cores and rims yielded a mean concordant age at 36.8 ± 0.4 Ma (n= 20;

MSWD for c+e = 1.2). This age suggests that the Mt. Ospedale tonalite pertain to the Adamello unit rather than to the older Corno Alto or Re di Castello unit.

8. Zircon geochemistry

8.1 Trace element compositions

Trace element composition was determined for some of the previously dated zircon domains and key compositional features are reported in figure 8. The full trace element characterisation is reported in Table C.2 and in Fig. D.4). A-type domains show chondrite-normalized (McDonough and Sun, 1995) REE patterns, characterized by HREE enrichment [$(Lu/Gd)_N$ > 26-100], positive Ce anomaly, and negative Eu anomaly (Eu/Eu* down to ~ 0.4). These domains also have relatively high Nb, Ta (up to 86 ppm and 18 ppm, respectively) and U contents (~ 750-5550 ppm) while their Th/U ratio is low (< 0.5). B-type domains have REE patterns characterized by higher ΣLREE contents, a less pronounced HREE enrichment [$(Lu/Gd)_N$ ~ 9-40], positive Ce anomaly, and absent or slightly negative Eu anomaly (Eu/Eu* ~ 0.7). The concentrations in Nb and Ta are very low (up to a maximum of 10 ppm and 2.2 ppm, respectively), and Th/U values range between 0.80 to 1.72.

8.2 Hf isotopic compositions

In-situ Hf isotope composition of magmatic zircons was carried out on selected previously dated domains (Fig. 9). Zircon grains from the TMG show considerable variation in $\varepsilon Hf_{(i)}$ (-3.2 to +14.1) with a multimodal distribution of data characterized by the occurrence of at least three dominant clusters at around +3, +8, and +13. Interestingly, the higher $\varepsilon Hf_{(i)}$ values pertain to the B-type textural zircon domains.

Zircon from the tonalitic rocks also have a large scatter in the $\varepsilon Hf_{(i)}$ isotopic composition, ranging between +2.5 and +13.0, with most of the values at ca. +6. The highest $\varepsilon Hf_{(i)}$ values are usually associated with B-type textural domains at the core of the grains (e.g., sample CA19-16, PTN). Noticeably, in sample CA19-21 (ETN), no $\varepsilon Hf_{(i)}$ values higher than +7 have been found.

The zircons from the EBGs show a more restricted variation in the $\varepsilon Hf_{(i)}$ isotopic compositions with most of values giving a nearly unimodal distribution at about +5. Few data gave lower and higher values (down to -2.5 and up to +9.1).

Most of the zircons from the MDR have $\varepsilon Hf_{(i)}$ values close to +6, with a few exceptions showing slightly negative value ($\varepsilon Hf_{(i)}$ down to -0.7). Noticeably, the old zircon core at 44 Ma shows $\varepsilon Hf_{(i)}$ at +12.0 ± 1.5 (2s). Negative $\varepsilon Hf_{(i)}$ values ranging from -3.2 to -9.6 are reported in the OTN sample.

9. Discussion

9.1 Is the Corno Alto complex peculiar in the Adamello batholith framework?

The Corno Alto and Sostino granitoids have been described in the literature as an association of granodiorite to trondhjemite rocks (Macera et al., 1983; Relvini et al., 2022; Schaltegger et al., 2019), with distinct mineralogical and chemical features from the rest of the Adamello Batholith.

Here, we show that none of the granitoids in the Corno Alto and Sostino unit is a trondhjemite according to the Ab-An-Or normative diagram. Moreover, considering all the available data in the literature on the Corno Alto and Sostino rocks, only a very restricted number of samples effectively fall in the compositional trondhjemite field, with the vast majority being instead granodiorites and tonalites (Fig. 3c). The Corno Alto rocks have however some peculiar petrographic and geochemical features relative to the other units of the batholith even if compared with rocks of similar age (e.g., south Re di Castello). Petrographically, the igneous epidote is almost ubiquitous in the Corno Alto rocks and occurs in place of amphibole which is the major mafic phase commonly found in the Adamello tonalite to granodiorite (e.g., Callegari & Brack, 2002). Noticeably, in the oldest EBG rocks from Sostino epidote occurs as inclusion into both plagioclase and biotite thus suggesting a crystallization at relatively high pressure (> 0.8 GPa; Schmidt & Poli 2004). Being the dissolution of epidote in granitic magmas a relatively fast process (e.g. Sial et al., 2008), its occurrence in low pressure rocks such as those of the Corno Alto implies a fast melt ascent. This is also consistent with the occurrence of centimetric oscillatory-zoned plagioclase phenocrysts displaying albite-rich poikilitic rims with tiny quartz inclusions, interpreted as evidence of an initial slow crystallization followed by fast-cooling and intrusion into cooler regions of the lithosphere during the final stages of crystallization.

The Corno Alto granitoids also have a distinctive chemical composition. These rocks represent the most differentiated products of the Adamello batholith (SiO_2 up to 72 wt.%) and show the most peraluminous compositions ($0.98 \leq A/CNK \geq 1.2$; Fig. 3b). Moreover, at any given SiO_2 content, the Corno Alto rocks have slightly higher Na_2O than most of the Adamello granitoids. Exception is made only for some

SiO_2-rich rocks from the Val Fredda Complex (Re di Castello unit) and W-Adamello (Blundy and Sparks, 1992; Dupuy et al., 1982; Macera et al., 1983; Ulmer et al., 1983). The trace element composition of the Corno Alto rocks reveals also peculiar features that include a strong Ba (Fig. 5), and to a minor extent Sr enrichment (Sr/Y > 40) and light-REE enrichment over HREE (La_N/Yb_N > 20) and Y, at any given SiO_2 content.

9.2 Timing of the assembly of the Corno Alto complex

The geochronological data presented in this work refine the current knowledge on the age of emplacement of the Corno Alto complex (Ji et al., 2019; Schaltegger et al., 2019) suggesting an assembly by multiple and possibly discrete magma injections in a time span of ~5 Ma (Fig. 7). U-Pb concordant data shows the occurrence of three main recurring age peaks at c. 44 Ma, c. 42 Ma, and c. 39 Ma (Fig. 10). The easternmost sector of the Corno Alto unit (Fig. 10a) exhibits the oldest ages with dates that are exclusively around ca. 44 Ma. These dates are equivalent to those reported by Schaltegger et al. (2019) and Ji et al. (2019) for the Corno Alto complex and likely represent the oldest igneous event in the Adamello batholith. The rocks dominating the central sector of the unit (Fig. 10c) show a relatively large age dispersion with a major peak at 42 Ma and a poorly defined inflection at 44 Ma. Noticeably, in the PTN sample the 42 Ma peak is statistically different from that at 44 Ma, which mostly results from the analysis of zircon cores (Fig 10.c2). In this sample, no age distinction was observed between the different zircon types recognised under cathodoluminescence. The 42 Ma peak is thus interpreted as a second distinct and younger magmatic pulse, which likely assembled the central sector of the Corno Alto complex. Here, the 44 Ma domains are interpreted as antecrysts (e.g., Miller et al., 2007) – *i.e.* zircon grains crystallized from earlier magmatic pulses and mechanically incorporated into the intruding magma during emplacement. The youngest age cluster at 39 Ma, which is also distinct from the event at 42 Ma, characterises the lithologies at the western border of the complex (Fig. 10e). The occurrence of antecryst zircons at 44 Ma suggests that also this younger event recycled previous intrusions. The widespread occurrence of several inherited zircon grains of Proterozoic to Paleozoic age suggests extensive interaction of the magma with a host basement constituted by metasedimentary rocks in agreement with Boriani & Giobbi-Origoni (1982).

The three magmatic pulses that assembled the Corno Alto complex are not distributed randomly but identify a trend of decreasing ages from the east to the west (Fig. 7). The progressive W-ward rejuvenation of the Corno Alto rocks could be interpreted as induced by partial resetting of the U-Pb zircon system in response to the emplacement of the younger western Adamello units (e.g., Re di Castello North and Adamello). However, this conflicts with the multiple zircon populations (also within a single rock sample) characterizing the central sector of the unit. Because the W-ward trend of decreasing U-Pb ages is roughly perpendicular to the direction of the Giudicarie Fault, which is located right above the European slab edge (Sun et al., 2019) possibly formed by tearing after interaction between the European and Dinaric slabs (Ji al., 2019; Malusà et al., 2021), we can thus identify a progressive migration of igneous activity in the Corno Alto complex away from the slab tear through time.

At the regional scale, it is noteworthy that the earliest magmatic events recorded in the Corno Alto rocks (at c. 44 Ma) also occur as xenocrystic zircon cores in the mafic rocks of the South Re di Castello unit (Tiepolo et al., 2011). This finding suggests that the onset of subduction-related igneous activity at 44 Ma in the Southern Alps was not restricted to the Corno Alto complex (D'Adda et al., 2011). It likely affected a wider crustal area, currently extending south-west towards the Val Fredda complex, paralleling the Giudicarie Fault and, thus, the trace of the European slab tear inferred on a geophysical ground (Malusà et al., 2021). In support of this conclusion is also the analogy in trace element composition and Hf isotopes of the B-type domains of the Corno Alto zircons with those of the Mt. Mattoni gabbro and Blumone hornblende-rich quartz diorite zircons (Broderick et al., 2015; Schoene et al., 2012), which strongly suggests a common origin. On the other hand, the A-type domains identified in the Corno Alto zircons also match the composition of the differentiated rocks of the Val Fredda complex, suggesting a common evolution with time of the entire crustal sector (Fig. 8). In this regard, the U-Pb ages of the Corno Alto and Val Fredda complexes fit the ages characterizing the youngest magmatic episodes of the intraplate Veneto Volcanic Province (VVP) in the Lessini Mts. and Val d'Adige, at ~51 Ma, ~45 Ma and ~42 Ma (Brombin et al., 2019; Visonà et al., 2007), which are also located along the inferred trace of the European slab tear.

9.3 Evidence for geochemically distinct sources at the origin of the Corno Alto complex

The granitoid rocks from the Corno Alto complex show the coexistence of at least two geochemically distinct components: i) a high Ba component characterized by high Sr and La/Yb ratios; ii) a juvenile component that crystallized high Ca plagioclase cores and zircon cores having $\varepsilon Hf_{(t)}$ signature approaching the depleted mantle.

The high Ba-La/Yb component

The SiO_2 > 60 wt% of the Corno Alto rocks, their Sr/Y > 40, and $(La/Yb)_N$ > 10 (Fig. 11a-b) roughly recall the geochemical signatures of a particular group of arc related melts known as adakites (Defand and Drummond, 1990). In particular, the Corno Alto rocks have major and trace element compositional features (i.e., mg# ≈ 0.5, Na_2O > 3.5%, K_2O/Na_2O ratios ≈ 0.4, Y <18, Yb <1.8 ppm and Sr >400 ppm) that fulfil the criteria used by Martin et al., (2005) to define high-SiO_2 adakites (HSA). However, the extremely high Ba and, to a minor extent, Sr contents (≈1900 and 1100 ppm, respectively) shown by the Corno Alto suite is not properly consistent with adakites but more closely resemble the geochemical signature of a particular group of Phanerozoic rocks called 'high Ba-Sr granites' (Fowler and Rollinson, 2012).

A key aspect in the interpretation of the high Ba (-Sr) signature of the Corno Alto rocks is relative to the discussion of the mechanism responsible for the decoupling between Ba and K. In fact, the studied rocks have higher Ba concentrations at any given K content with respect to all the other Adamello rocks (Fig. 11c). Fractional crystallisation of plagioclase and/or biotite, which are the main minerals in the studied rocks, does not account for the Ba-K decoupling indicating that an external source for the Ba (and Sr) enrichment is thus required.

A multi-stage process of dehydration melting (and extraction of anatectic melts) of granulite-facies paragneiss was suggested by Sinigoi et al. (1994) to account for the high Ba and low K-Rb concentrations in the diorites of the Mafic Complex in the Ivrea Verbano Zone. The progressive breakdown of biotite with the production of garnet-bearing restitic assemblages would have been responsible for the Ba-K decoupling. Relvini et al. (2022) also suggested in the petrogenesis of the Corno Alto rocks an input from anatectic melts from metapelites in the lower crust. However, residual garnet in the residue, even in low proportions, contrasts with the spoon-shaped HREE pattern and the low Gd/Yb ratios of the Corno Alto rocks. We also exclude that the shallow level contamination is the main source of the high Sr, Ba and La/Yb ratios of the

Corno Alto rocks because the low-grade Variscan host basement (Rendena Schists) does not possess high Ba contents (Bigazzi et al., 1986) and high La/Yb ratios.

The Ba (and Sr) enrichment relative to K is likely a primary feature of the parental melt inherited from the mantle source. Partial melting of a metasomatized phlogopite-bearing mantle wedge would generate Ba and K-rich melts (Fowler et al., 2008). The K and Ba decoupling is accomplished only by involving minerals strongly discriminating elements by charge, i.e., capable of preferentially accept large 2+ cations (e.g., Ba^{2+} and Sr^{2+}) rather than 1+ cations (e.g., K^{+}) such as carbonates or sulphates. Pelagic sediments were reported to be possibly extremely rich in Ba and Sr and also LREE-enriched (e.g., Fowler et al., 2008; Plank and Langmuir, 1998). Barium and Sr in pelagic sediments are notably linked to biological productivity (i.e., barite precipitation) and biogenic phases (i.e., Sr in biogenic carbonates). Strontium is particularly abundant in Cenozoic carbonate oozes (up to 1500-2000 ppm) while it is relatively low in average shales (150-200 ppm). High Ba concentrations characterize proximal hydrothermal sediments where barite is commonly present, and sediments related to high biological productivity where barite is in association with organic matter and siliceous plankton (Plank, 2014).

In figure 12a the Ba-Sr composition of the Corno Alto rocks is compared with that of several key drilled sections of present-day near deep-trenches worldwide, having different proportions of the diverse sedimentary constituents (Plank, 2014). The Corno Alto rocks are highly different from the pelitic- and terrigenous-dominated subducting trenches (e.g., Aleutians, Kermadec, Sandwich) and define a trend pointing to the composition of a carbonate sediment cover of the slab (e.g., Columbia subducting trench). The Corno Alto rocks, in particular, parallel the Kermadec subducting sediment trench, which is characterized by high proportions of carbonate material and noticeably closely resembles the composition of the Penninic units of the Tauern Window in the Eastern Alps (Fig. 12b-1 and 12b-2; Kurz et al., 1998). All the above pieces of evidence strongly suggest that the Ba enrichment shown by the Corno Alto rocks is related to the involvement of a carbonate-rich component in the source, as expected for the sediments deposited on top of the Neo-Tethyan oceanic crust.

To constrain the petrogenesis of the high Ba-La/Yb component, a process capable to produce both the Ba enrichment and the La/Yb fractionation is required. Experimental studies indicate that Ba (and Sr) is highly soluble in the fluid phase (e.g., Kessel et al., 2005) compared to REE that are more prone to be retained in the solid residue of the slab. The presence of Cl in the system may enhance the mobility of several trace elements, including REE (e.g., Rustioni et al., 2021). However, being marine carbonates a Cl-poor system (e.g., Wang et al., 2020), the involvement of silicate hydrous melts or supercritical fluids is required for the REE transfer (Kessel et al., 2005; Fowler and Rollinson, 2012; Hermann and Rubatto, 2009).

The juvenile component

Evidence for the occurrence of a juvenile component into the petrogenesis of the Corno Alto rocks comes from trace element and *in-situ*-Hf isotopes. Zircon in the 44 Ma Sostino and ETN rocks are characterized by A-type textures and $\varepsilon Hf_{(t)}$ values close to +6 (±0.5 2SE). Zircon grains in all the other lithologies reveal multiple domains with both A-type and B-type (Fig. 6). $\mathcal{E}Hf_{(t)}$ values in A-Type domains are identical to those observed in the older rocks. B-type domains instead have highly positive $\mathcal{E}Hf_{(t)}$ values (up to +14), low incompatible elements concentrations (e.g., U, Nb, Ta) and a weak Eu anomaly, all features suggesting crystallisation from a juvenile melt whose $\varepsilon Hf_{(t)}$ is close to that of DM (Vervoort and Kemp, 2016). Noticeably, B-type domains are always at the core of the crystals and show resorption boundaries. Some B-type domains yield dates clearly older than the rim (e.g., MDR sample), in other cases the difference in age is below the analytical capability of the applied technique. In any case, the resorption boundary characterising B-type domains is evidence for their xenocrystic origin (Fig. 6). We thus suggest that at 44 Ma mantle-derived melts with a $\mathcal{E}Hf_{(t)}$ signature close to MORB, crystallised at depth and were lately (42-39 Ma) recycled by younger igneous pulses. This is also in agreement with our finding of corroded An_{90} domains at the core of more albitic plagioclase crystals. Noticeably this process was already reported in the evolved rocks of the Re di Castello unit (Blundy and Shimizu, 1991). A-type domains, with high incompatible elements concentrations and deep negative Eu anomaly, likely crystallised from the same parental melt but after melt differentiation by fractional crystallisation and assimilation of the shallow crust (e.g., Relvini et al., 2021) which is likely characterised by lower $\mathcal{E}Hf_{(t)}$.

9.4 Constraints on melt generation and geodynamic implications

The Corno Alto is the oldest intrusive complex of the entire Alpine Orogen (Ji et al., 2019) and represents the onset of the igneous activity. The Corno Alto complex has thus particular importance in the interpretation of the geodynamic evolution of the Alps. Many models were proposed to account for the long-lasting absence of magmatic activity during the Alpine Tethys subduction, whose beginning is approximately set at ~100‐95 Ma (e.g., Dewey et al., 1989; Malusà et al. 2015; Agard, 2021, and reference therein). Most of these models agree on the absence of sufficient fluids to promote partial melting in the mantle wedge (Agard, 2021). This is consistent with the reconstructed cold path of Alpine subduction, very close to the so-called forbidden zone, as recorded by exhumed (U)HP rocks (Malusà et al. 2015). This evidence is reinforced by exhumed alpine high-P and ultrahigh-P metasedimentary rocks still retaining most of their volatile fraction (Busigny et al., 2003; Bebout et al., 2013; Garofalo, 2012). The onset of magmatism at 44 Ma, was likely triggered by the thermal perturbation induced by rising asthenospheric material along the slab tear located beneath the area encompassing the Adamello batholith, the Veneto Volcanic Province and the Giudicarie Fault, and was subsequently sustained by a corner flow of asthenospheric material during progressive slab steepening (Ji et al., 2019). Brombin et al., (2021) invoked a mechanism of asthenospheric poloidal flow to account for the middle Eocene magmatism in the Veneto Volcanic Province (VVP; NE Italy).

In this study, we showed that the parental melts of the Corno Alto complex record the presence of a component derived from the subducted carbonates, which is not occurring in all the younger units of the batholith. This evidence is essential in the interpretation of the evolution of the Alpine subduction because it implies a change with time in the sources activated for magma production. The loss of the carbonate input after 41 Ma may be accounted for by a change in the composition of the subducted material or, alternatively in the mechanism responsible for the element transfer from the slab to the mantle wedge.

The Alpine Tethys seafloor consisted of a complex assemblage of variably refertilized exhumed mantle rocks, irregularly distributed mafic magmatic rocks and pelagic sediments, together with ocean-continent transition lithosphere (OCT) domains and extensional allochthons (Malusà et al. 2018; Agard 2021). The slab compositional heterogeneities could therefore account for a sporadic carbonate input into the mantle wedge. However, the carbonate input does not recur in the younger units of the Adamello batholith as would be expected during the subduction of a compositionally heterogenous slab. Alternatively, being melt production very close to the onset of continental collision in the Central Alps after complete consumption of the Tethyan oceanic basin (e.g., Agard, 2021). Palinspastic reconstructions of the Alpine region consistently show that the inception of continental subduction migrated progressively from the Western to the Central Alps (Ford et al., 2006; Malusà et al., 2015), with the OCT lithosphere reaching the trench at ca 50-45 Ma (Malusà et al., 2018; Ji et al. 2019). Therefore, the formation of the Corno Alto marks the transition from oceanic subduction to the beginning of OCT subduction. In this scenario, the OCT subduction may lead to an increase in the terrigenous components in the subducting material, with this increase that should be clearly visible in the chemistry of the produced melts. A similar model was proposed by Tiepolo et al., (2014) that ascribed the difference in the chemistry between the amphibole-rich mafic rocks of the Adamello (Mt. Mattoni) and Bergell intrusions to differences in the composition of the subducting lithosphere. In particular, the enrichment in elements with high crustal affinity and the lower $\varepsilon Hf_{(t)}$ signature characterising the Bergell primary melts was related to the subduction of a thinned continental lithosphere. In the Adamello batholith the recognition of a terrigenous input in the source is difficult to assess mostly due to the superimposed effect of shallow level crustal contamination. Despite this limitation, we reckon that the similar Th/Nb ratio exhibited by these rocks of the Corno Alto system and younger Adamello units of similar composition suggests that no significant changes in the terrigenous input have occurred (Plank, 2005).

The carbonate input characterizing the Corno Alto rocks is likely a consequence of a mechanism of element transfer from the slab to the mantle wedge, active only at the onset of the magmatism at 44 Ma. The thermal perturbation in response to the rise of asthenospheric material was particularly important near the torn edge of the European slab where the Corno Alto pluton is roughly located (Ji et al., 2019). Recent experiments revealed that under hydrous conditions temperatures in the range 850 – 900 °C at 4.2 – 6 GPa (pertaining to warm subduction thermal conditions; Syracuse et al., 2010), may enhance partial melting of the carbonate fraction (Schettino and Poli, 2020). We thus propose that the high thermal conditions, in response to the asthenosphere upwelling, locally induced partial melting of the carbonate fraction of the sediment cover of the slab. Low-degree melting of carbonated sediments of slab origin were documented to be responsible of the strong enrichment in LREE of the mantle under the north China Craton (Chen et al., 2017). Carbonate melting thus can account also for the relatively high La/Yb ratios characterizing the Corno Alto melts. Interestingly, Zaccaria et al. (2021) found in the melt inclusions into zircon megacrysts of the middle Eocene VVP enrichments in BaO - SrO and evidence for S, and CO_2-rich fluids that were correlated to a source metasomatized by carbonatitic-kimberlitic liquids. The stringent analogy with the geochemical peculiarities found in the Corno Alto complex suggests a genetic link between the two complexes that is worth of detailed future investigations.

The high thermal conditions suitable for carbonate melting lasted approximately 5 Ma and were possibly at the origin of melts with adakitic signature reported in the Re di Castello unit (e.g., Tiepolo and Tribuzio, 2005). With the progressive lowering of the thermal conditions, slab dehydration become the dominant mechanism of element transfer from the slab to the mantle wedge. Being carbonate Hf-free, carbonate melting does not affect the $\varepsilon Hf_{(t)}$ signature of the mantle derived melts. We thus interpret the depleted $\varepsilon Hf_{(t)}$ signature found in the Corno Alto and approaching that of MORB (Vervoort et al., 2011), as reflecting the DM nature of the mantle source. Likely all the lower $\varepsilon Hf_{(t)}$ values found in zircon of the evolved Corno Alto lithologies reflect at various extent shallow level crustal contamination. Noticeably, depleted $\varepsilon Hf_{(t)}$ signatures also characterise zircons from the slightly younger products (39-41 Ma) of the southern Adamello (Ji et al., 2019; Schaltegger et al., 2019; Tiepolo et al., 2011), implying that no significant changes in the mantle source region have occurred. A larger scale mantle source homogeneity is also testified by the occurrence of a DM signature in the igneous products of the VVP (Beccaluva et al., 2007; Bianchini et al., 2008) and interpreted as the mantle signature prior the subduction-related metasomatism (Brombin et al., 2019). This is further evidence for common inputs of deep asthenospheric mantle material in the source regions of the oldest Adamello products and the VVP (Fig. 13).

10. Concluding remarks

The peculiar petrogenetic processes found at the origin of the Corno Alto complex suggest an alternative model for the petrogensis of the high Ba/K sanukitoids, which has implications for understanding the compositional transition between the Archean and the post-Archean granitoids. The petrogenesis of the Corno Alto complex has been traced back to a carbonate input in the source which transfers to the melt its distinctive high Ba/K ratio by hydrous-melts or supercritical fluids. The key factors for this process are thus a carbonate source of the metasomatic agent and the availability of thermal conditions high enough for the carbonate partial melting. During Early Archean, although thermal conditions were sufficient for carbonate melting, carbonate inputs in subducting systems was almost negligible due to the paucity of carbonate marine organism (Veizer & McKenzie, 2003; Ernst, 2009). Carbonate platforms began to appear during the late Archean but have become increasingly widespread since the Proterozoic and Phanerozoic when subduction thermal conditions do not reach the temperatures necessary for carbonate melting (Laurent et al., 2011). It follows that the full accomplishment of the conditions required for the genesis of the high Ba/K granitoids is mostly found at the Archean-Proterozoic transition.

In conclusion, the anomalous thermal conditions (in the range of 850 – 900 °C at 4.2 – 6 GPa) pertaining to the Alpine subduction at 44 Ma apparently parallel those at the Archean-Proterozoic transition. The Corno Alto suite, as well as other Ba-Sr granites (Fowler and Rollinson, 2012) could thus represent a kind of modern analogues of the high Ba/K sanukitoids.

CAPTIONS TO FIGURES

Figure 1. a-b) Modified from Ji et al., (2019); c) Modified from Schaltegger et al. (2009); d) Modified from Carta geologica Provincia autonoma di Trento – Dati elaborati dal Servizio Geologico della provincia Autonoma di Trento (Sez. N. 59050-59010-59090).

Figure 2. a) Two plagioclase crystals of type 1 in TMG; b) Plagioclase glomerocryst in TMG; c) Epidote crystal enclosed in plagioclase in TMG; d) Lamellar primary white mica in TMG; e) big oscillatory zoned plagioclase in PTN; f) Tiny quartz crystals enclosed in the rim of plagioclase phenocrysts in PTN; g) Epidote euhedral inclusion in biotite in ETN; (h) Epidote overgrowth on allanite grains in ETN; i) Euhedral epidote grains in EBG.

Figure 3. a) A/CNK (A/CNK = Al / (2 Ca + Na + K) expressed as molar proportion atoms) vs. A/NK (A/NK = Al /(Na + K) expressed as molar proportion atoms) b) MALI index ([Na_2O + K_2O] - CaO) vs. SiO_2 diagram; c) Normative An-Ab-Or diagram (after Barker, 1979) for Corno Alto plutonic rocks. d) Ternary K-Na-Ca plot. The classification curves are from Barker & Arth (1976). Literature data are SiO_2-rich Adamello

rocks with SiO_2 > 56 wt.% (data from: Dupuy et al., 1982; Macera et al., 1983; Kagami et al., 1991; Blundy & Sparks, 1992; Ji et al., 2019; Relvini et al., 2022).

Figure 4. Major-element geochemistry of the Corno Alto and Sostino rocks compared with literature data (same as in figure 3).

Figure 5. Trace element composition of the Corno Alto rocks compared to the other Adamello rocks (the dashed patterns define the SiO_2-rich Adamello rocks with SiO_2 > 56 wt.%); symbols are the same of Fig. 3. a) Multi-element patterns normalized to Primitive Mantle (McDonough and Sun, 1995); b) Ba (ppm) vs. Sr (ppm) diagram for the Corno Alto rocks (coloured dots) and the other Adamello rocks (grey dots).

Figure 6. Cathodoluminescence images of representative zircon grains from the Corno Alto unit. U–Pb and εHf errors are reported as 2s.

Figure 7. Compilation of weighted average ages of zircon from the Corno Alto complex by laser-ablation ICP-MS. Error are reported as 2SE.

Figure 8. Hf (ppm) *vs*. $(Lu/Gd)_N$ and Th/U *vs*. Eu/Eu^* diagrams from the Corno Alto zircons compared to Val Fredda (grey dots; Broderick et al. 2015) and the Veneto Volcanic Province (VVP) zircon crystals (green dots; from Visonà et al. 2007). Errors are within symbol.

Figure 9. Single zircon dates and Hf isotopes compositions from the Corno Alto and Mt. Ospedale rocks.

Figure 10. On left in image, geochronological results (U-Pb concordant data) for the Corno Alto rocks from the eastern (a), central (c) and western (e) parts of the Complex. On the right (b, d, f), distribution of $\varepsilon Hf_{(t)}$ values in zircon grains from the same rocks. Errors for Hf are reported as 2s.

Figure 11. Chondrite normalized (McDonough and Sun, 1995) $(La/Yb)_N$ vs. Yb_N (a) and Sr/Y vs. Y (ppm) (b) diagrams for the Corno Alto granitoids compared with classical island arc (light grey, Martin, 1999) and adakite fields (dark grey, Defant and Drummond, 1990); c) Ba (ppm) vs K_2O (wt.%) diagram showing the Ba-K decoupling for the Corno Alto rocks compared to literature data.

Figure 12.a) Ba/Sr ratio vs. Ba ppm for the Corno Alto rocks and bulk estimates for some complete sections near deep-trenches from all around the world (data from Plank, 2014). Grey field reports the variability of other Adamello rocks; b-1) Summary lithology subducting at each considered trench modified from Plank (2014); b-2) Representative stratigraphic section for the Tauern Window (modified after Kurz et al., 1998). Symbols are the same of Figure 11.

Figure 13. Modified from Ji et al., (2019). 3-D model showing the proposed relationships between slab steepening and Corno Alto magmatism (CA) in the absence of slab breakoff. The model highlight the influx of the high Ba-La/Yb component deriving from subducted carbonate sediments. Projection of the Veneto Volcanic Province (VVP) is also shown (see text for details).

11. References 79/80

Agard, P., 2021. Subduction of oceanic lithosphere in the Alps: Selective and archetypal from (slow-spreading) oceans. Earth-Science Rev. 214, 103517. https://doi.org/10.1016/j.earscirev.2021.103517

Barker, F., Arth, J.G., Millard Jr, H.T., 1979. Archean trondhjemites of the southwestern Big Horn Mountains, Wyoming: a preliminary report, in: Developments in Petrology. Elsevier, pp. 401–414.

Barker, F., 1979. Chapter 1 - Trondhjemite: Definition, Environment and Hypotheses of Origin, in: BARKER, F.B.T.-D. in P. (Ed.), Trondhjemites, Dacites, and Related Rocks. Elsevier, pp. 1–12. https://doi.org/https://doi.org/10.1016/B978-0-444-41765-7.50006-X

Bebout, G.E., Agard, P., Kobayashi, K., Moriguti, T., Nakamura, E., 2013. Devolatilization history and trace element mobility in deeply subducted sedimentary rocks: Evidence from Western Alps HP/UHP suites. Chem. Geol. 342, 1–20. https://doi.org/10.1016/j.chemgeo.2013.01.009

Beccaluva, L., Bianchini, G., Bonadiman, C., Coltorti, M., Milani, L., Salvini, L., Siena, F., Tassinari, R., 2007. Intraplate lithospheric and sublithospheric components in the Adriatic domain: Nephelinite to tholeiite magma generation in the Paleogene Veneto volcanic province, southern Alps. Spec. Pap. Geol. Soc. Am. 418, 131–152. https://doi.org/10.1130/2007.2418(07)

Bianchini, G., Beccaluva, L., Siena, F., 2008. Post-collisional and intraplate Cenozoic volcanism in the rifted Apennines/Adriatic domain. Lithos 101, 125–140. https://doi.org/10.1016/j.lithos.2007.07.011

Bigazzi, G., Del Moro, A., Macera, P., 1986. A quantitative approach to trace element and Sr isotope evolution in the Adamello batholith (northern Italy). Contrib. to Mineral. Petrol. 94, 46–53.

Blanckenburg, F. Von, Davies, J.H., 1995. Slab breakoff: a model for syncollisional magmatism and tectonics in the Alps. Tectonics 14, 120-131.

Blundy, J.D., Sparks, R.S.J., 1992. Petrogenesis of mafic inclusions in granitoids of the adamello massif, Italy. J. Petrol. 33, 1039–1104. https://doi.org/10.1093/petrology/33.5.1039

Blundy, J.D., Shimizu, N., 1991. Trace element evidence for plagioclase recycling in calc-alkaline magmas. Earth Planet. Sci. Lett. 102, 178–197. https://doi.org/10.1016/0012-821X(91)90007-5

Boriani, A., Giobbi Origoni, E., 1982. Heat transfer in the thermo-metamorphic aureola of the northeastern sector of Mt. Adamello (Trento-Italy). Rend. SIMP 38, 3, 1251-1360.

Broderick, C., Wotzlaw, J.-F., Frick, D., Gerdes, A., Ulianov, A., Günther, D., Schaltegger, U., 2015. Linking the thermal evolution and emplacement history of an upper‐ crustal pluton to its lower‐ crustal roots using zircon geochronology and geochemistry (southern Adamello batholith, N. Italy). Contrib. to Mineral. Petrol. 170. https://doi.org/10.1007/s00410-015-1184-x

Brombin, V., Bonadiman, C., Jourdan, F., Roghi, G., Coltorti, M., Webb, L.E., Callegaro, S., Bellieni, G., De Vecchi, G., Sedea, R., Marzoli, A., 2019. Intraplate magmatism at a convergent plate boundary: The case of the Cenozoic northern Adria magmatism. Earth-Science Rev. 192, 355–378. https://doi.org/10.1016/j.earscirev.2019.03.016

Brombin, V., Pettitt, E.A., Fahnestock, M.F., Casalini, M., Webb, L.E., Bryce, J.G., Bianchini, G., 2021. New geochemical and geochronological data on the Cenozoic Veneto Volcanic Province: Geodynamic inferences. Lithos 406–407, 106507. https://doi.org/10.1016/j.lithos.2021.106507

Busigny, V., Cartigny, P., Philippot, P., Ader, M., Javoy, M., 2003. Massive recycling of nitrogen and other fluid-mobile elements (K, Rb, Cs, H) in a cold slab environment: Evidence from HP to UHP oceanic metasediments of the Schistes Lustrés nappe (western Alps, Europe). Earth Planet. Sci. Lett. 215, 27–42. https://doi.org/10.1016/S0012-821X(03)00453-9

Callegari, E., Brack, P., 2002. Geological map of the Tertiary Adamello Batholitih (Northern Italy). Mem. di Sci. Geol. Padova 54, 19–49.

Chen, C., Liu, Y., Foley, S.F., Ducea, M.N., Geng, X., Zhang, W., Xu, R., Hu, Z., Zhou, L., Wang, Z., 2017. Carbonated sediment recycling and its contribution to lithospheric refertilization under the northern North China Craton. Chem. Geol. 466, 641–653. https://doi.org/10.1016/j.chemgeo.2017.07.016

D'Adda, P., Zanchi, A., Bergomi, M., Berra, F., Malusà, M.G., Tunesi, A., Zanchetta, S., 2011. Polyphase thrusting and dyke emplacement in the central Southern Alps (Northern Italy). Int. J. Earth Sci. 100, 1095–1113. https://doi.org/10.1007/s00531-010-0586-2

Defant, M.J., Drummond, M.S., 1990. Derivation of some modern arc magmas by melting of young subducted lithosphere. Nature 367, 662-665.

Dewey, J.F., Helman, M.L., Knott, S.D., Turco, E., Hutton, D.H.W., 1989. Kinematics of the western Mediterranean. Geol. Soc. London, Spec. Publ. 45, 265–283.

Dupuy, C., Dostal, J., Fratta, M., 1982. Geochemistry of the Adamello Massif (Northern Italy). Contrib. to Mineral. Petrol. 80, 41–48. https://doi.org/10.1007/BF00376733

Ernst, W.G., 2009. Archean plate tectonics, rise of Proterozoic supercontinentality and onset of regional, episodic stagnant-lid behavior. Gondwana Res. 15, 243–253.

Fisher, C.M., Vervoort, J.D., Dufrane, S.A., 2014. Accurate Hf isotope determinations of complex zircons using the "laser ablation split stream" method. Geochemistry, Geophys. Geosystems 15, 121–139. https://doi.org/10.1002/2013GC004962

Foley, S., Tiepolo, M., Vannucci, R., 2002. Growth of early continental crust controlled by melting of amphibolite in subduction zones. Nature 417, 837–840. https://doi.org/10.1038/nature00799

Ford, M., Duchêne, S., Gasquet, D., Vanderhaeghe, O., 2006. Two-phase orogenic convergence in the external and internal SW Alps. J. Geol. Soc. London. 163, 815–826.

Fowler, M., Rollinson, H., 2012. Phanerozoic sanukitoids from Caledonian Scotland: Implications for Archean subduction. Geology 40, 1079–1082. https://doi.org/10.1130/G33371.1

Fowler, M.B., Kocks, H., Darbyshire, D.P.F., Greenwood, P.B., 2008. Petrogenesis of high Ba-Sr plutons from the Northern Highlands Terrane of the British Caledonian Province. Lithos 105, 129–148. https://doi.org/10.1016/j.lithos.2008.03.003

Garofalo, P.S., 2012. The composition of Alpine marine sediments (Bündnerschiefer Formation, W Alps) and the mobility of their chemical components during orogenic metamorphism. Lithos 128–131, 55–72. https://doi.org/10.1016/j.lithos.2011.10.009

Griffin, W., Powell, W., Pearson, N.J., O'Reilly, S., 2008. GLITTER: data reduction software for laser ablation ICP-MS. Short Course Ser. 40, 308-311.

Hawkesworth, C.J., Cawood, P.A., Dhuime, B., 2020. The Evolution of the Continental Crust and the Onset of Plate Tectonics. Front. Earth Sci. 8, 1–23. https://doi.org/10.3389/feart.2020.00326

Hermann, J., Rubatto, D., 2009. Accessory phase control on the trace element signature of sediment melts in subduction zones. Chem. Geol. 265, 512–526. https://doi.org/10.1016/j.chemgeo.2009.05.018

Hogan, J.P., 1993. Monomineralic glomerocrysts: textural evidence for mineral resorption during crystallization of igneous rocks. J. Geol. 101, 531–540. https://doi.org/10.1086/648245

Ji, W.Q., Malusà, M.G., Tiepolo, M., Langone, A., Zhao, L., Wu, F.Y., 2019. Synchronous Periadriatic magmatism in the Western and Central Alps in the absence of slab breakoff. Terra Nov. https://doi.org/10.1111/ter.12377

Jochum, K.P., Weis, U., Stoll, B., Kuzmin, D., Yang, Q., Raczek, I., Jacob, D.E., Stracke, A., Birbaum, K., Frick, D.A., 2011. Determination of reference values for NIST SRM 610–617 glasses following ISO guidelines. Geostand. Geoanalytical Res. 35, 397–429.

Jochum, K.P., Weis, U., Schwager, B., Stoll, B., Wilson, S.A., Haug, G.H., Andreae, M.O., Enzweiler, J., 2016. Reference Values Following ISO Guidelines for Frequently Requested Rock Reference Materials. Geostand. Geoanalytical Res. 40, 333–350. https://doi.org/10.1111/j.1751-908X.2015.00392.x

Kagami, H., Ulmer, P., Hansmann, W., Dietrich, V., Steiger, R.H., 1991. Nd-Sr isotopic and geochemical characteristics of the southern Adamello (northern Italy) intrusives: Implications for crustal versus mantle origin. Journal of Geophysical Research: Solid Earth 96, B9, 14331-14346.

Kessel, R., Schmidt, M.W., Ulmer, P., Pettke, T., 2005. Trace element signature of subduction-zone fluids, melts and supercritical liquids at 120-180 km depth. Nature 437, 724–727. https://doi.org/10.1038/nature03971

Kurz, W., Neubauer, F., Genser, J., & Dachs, E., 1998. Alpine geodynamic evolution of passive and active continental margin sequences in the Tauern Window (eastern Alps, Austria, Italy): a review. Geologische rundschau, 87, 225-242.

Laubscher, H., 2010. Jura, Alps and the boundary of the Adria subplate. Tectonophysics 483, 223–239. https://doi.org/10.1016/j.tecto.2009.10.011

Laurent, O., Martin, H., Doucelance, R., Moyen, J.F., Paquette, J.L., 2011. Geochemistry and petrogenesis of high-K “sanukitoids” from the Bulai pluton, Central Limpopo Belt, South Africa: Implications for geodynamic changes at the Archaean-Proterozoic boundary. Lithos 123, 73–91. https://doi.org/10.1016/j.lithos.2010.12.009

Laurent, O., Martin, H., Moyen, J.F., Doucelance, R., 2014. The diversity and evolution of late-Archean granitoids: Evidence for the onset of “modern-style” plate tectonics between 3.0 and 2.5 Ga. Lithos 205, 208–235. https://doi.org/10.1016/j.lithos.2014.06.012

Lustrino, M., Duggen, S., Rosenberg, C.L., 2011. The Central-Western Mediterranean: Anomalous igneous activity in an anomalous collisional tectonic setting. Earth-Science Rev. 104, 1–40. https://doi.org/10.1016/j.earscirev.2010.08.002

Macera, P., G., F., A., P., E., C., 1983. A geochemical study on the acid and basic rocks of the Adamello batholith. Mem. Soc. Geol. It. 26, 223–259.

Malusà, M.G., Faccenna, C., Baldwin, S.L., Fitzgerald, P.G., Rossetti, F., Balestrieri, M.L., Danišík, M., Ellero, A., Ottria, G., Piromallo, C., 2015. Contrasting styles of (U) HP rock exhumation along the Cenozoic Adria- Europe plate boundary (Western Alps, Calabria, Corsica). Geochemistry, Geophys. Geosystems 16, 1786–1824.

Malusà, M.G., Frezzotti, M.L., Ferrando, S., Brandmayr, E., Romanelli, F., Panza, G.F., 2018. Active carbon sequestration in the Alpine mantle wedge and implications for long-term climate trends. Sci. Rep. 8, 4740.

Malusà, M.G., Guillot, S., Zhao, L., Paul, A., Solarino, S., Dumont, T., Schwartz, S., Aubert, C., Baccheschi, P., Eva, E., 2021. The deep structure of the Alps based on the CIFALPS seismic experiment: A synthesis. Geochemistry, Geophys. Geosystems 22, e2020GC009466.

Martin, H., Smithies, R.H., Rapp, R., Moyen, J.F., Champion, D., 2005. An overview of adakite, tonalite-trondhjemiten-granodiorite (TTG), and sanukitoid: Relationships and some implications for crustal evolution. Lithos 79, 1–24. https://doi.org/10.1016/j.lithos.2004.04.048

Martin, H., 1999. Adakitic magmas: Modern analogues of Archaean granitoids. Lithos 46, 411–429. https://doi.org/10.1016/S0024-4937(98)00076-0

McDonough, W.F., Sun, S. s., 1995. The composition of the Earth. Chem. Geol. 120, 223–253. https://doi.org/10.1016/0009-2541(94)00140-4

Miller, J.S., Matzel, J.E.P., Miller, C.F., Burgess, S.D., Miller, R.B., 2007. Zircon growth and recycling during the assembly of large, composite arc plutons. J. Volcanol. Geotherm. Res. 167, 282–299. https://doi.org/10.1016/j.jvolgeores.2007.04.019

Plank, T., Langmuir, C.H., 1998. The chemical composition of subducting sediment and its consequences for the crust and mantle. Chem. Geol. 145, 325–394. https://doi.org/10.1016/S0009-2541(97)00150-2

Plank, T., 2005. Constraints from Thorium/Lanthanum on sediment recycling at subduction zones and the evolution of the continents. J. Petrol. 46, 921–944. https://doi.org/10.1093/petrology/egi005

Plank, T., 2014. The Chemical Composition of Subducting Sediments, 2nd ed, Treatise on Geochemistry: Second Edition. Elsevier Ltd. https://doi.org/10.1016/B978-0-08-095975-7.00319-3

Rapp, R.P., Shimizu, N., Norman, M.D., 2003. Growth of early continental crust by partial melting of eclogite. Nature 425, 605–609. https://doi.org/10.1038/nature02031

Relvini, A., Martin, S., Carvalho, B.B., Prosser, G., Toffolo, L., Macera, P., Bartoli, O., 2022. Genesis of the Eastern Adamello Plutons (Northern Italy): Inferences for the Alpine Geodynamics. Geosci. 12. https://doi.org/10.3390/geosciences12010013

Rustioni, G., Audetat, A., Keppler, H., 2021. The composition of subduction zone fluids and the origin of the trace element enrichment in arc magmas. Contrib. to Mineral. Petrol. 176, 1–19. https://doi.org/10.1007/s00410-021-01810-8

Schaltegger, U., Brack, P., Ovtcharova, M., Peytcheva, I., Schoene, B., Stracke, A., ... & Bargossi, G. M. (2009). Zircon and titanite recording 1.5 million years of magma accretion, crystallization and initial cooling in a composite pluton (southern Adamello batholith, northern Italy). Earth and Planetary Science Letters, 286(1-2), 208-218.

Schaltegger, U., Nowak, A., Ulianov, A., Fisher, C.M., Gerdes, A., Spikings, R., Whitehouse, M.J., Bindeman, I., Hanchar, J.M., Duff, J., Vervoort, J.D., Sheldrake, T., Caricchi, L., Brack, P., Müntener, O., 2019. Zircon Petrochronology and 40Ar/39Ar Thermochronology of the Adamello Intrusive Suite, N. Italy: Monitoring the Growth and Decay of an Incrementally Assembled Magmatic System. J. Petrol. 60, 701–722. https://doi.org/10.1093/petrology/egz010

Schettino, E., Poli, S., 2020. Hydrous Carbonatitic Liquids Drive CO2 Recycling From Subducted Marls and Limestones. Geophys. Monogr. Ser. 249, 209–221. https://doi.org/10.1002/9781119508229.ch18

Schmidt, M.W., Poli, S., 2004. Magmatic epidote. Rev. Mineral. Geochemistry 56, 399–430. https://doi.org/10.2138/gsrmg.56.1.399

Schoene, B., Schaltegger, U., Brack, P., Latkoczy, C., Stracke, A., Günther, D., 2012. Rates of magma differentiation and emplacement in a ballooning pluton recorded by U-Pb TIMS-TEA, Adamello batholith, Italy. Earth Planet. Sci. Lett. 355–356, 162–173. https://doi.org/10.1016/j.epsl.2012.08.019

Shirey, S.B., Hanson, G.N., 1984. Mantle-derived Archaean monozodiorites and trachyandesites. Nature 310, 222–224. https://doi.org/10.1038/310222a0

Sial, A.N., Vasconcelos, P.M., Ferreira, V.P., Pessoa, R.R., Brasilino, R.G., Morais Neto, J.M., 2008. Geochronological and mineralogical constraints on depth of emplacement and ascencion rates of epidote-bearing magmas from northeastern Brazil. Lithos 105, 225–238. https://doi.org/10.1016/j.lithos.2008.04.002

Sinigoi, S., Quick, J.E., Clemens- Knott, D., Mayer, A., Demarchi, G., Mazzucchelli, M., Negrini, L., Rivalenti, G., 1994. Chemical evolution of a large mafic intrusion in the lower crust, Ivrea- Verbano Zone, northern Italy. J. Geophys. Res. Solid Earth 99, 21575–21590.

Sláma, J., Košler, J., Condon, D.J., Crowley, J.L., Gerdes, A., Hanchar, J.M., Horstwood, M.S.A., Morris, G.A., Nasdala, L., Norberg, N., Schaltegger, U., Schoene, B., Tubrett, M.N., Whitehouse, M.J., 2008. Plešovice zircon - A new natural reference material for U-Pb and Hf isotopic microanalysis. Chem. Geol. 249, 1–35. https://doi.org/10.1016/j.chemgeo.2007.11.005

Sun, W., Zhao, L., Malusà, M.G., Guillot, S., Fu, L.Y., 2019. 3-D Pn tomography reveals continental subduction at the boundaries of the Adriatic microplate in the absence of a precursor oceanic slab. Earth Planet. Sci. Lett. 510, 131–141. https://doi.org/10.1016/j.epsl.2019.01.012

Syracuse, E.M., van Keken, P.E., Abers, G.A., Suetsugu, D., Bina, C., Inoue, T., Wiens, D., Jellinek, M., 2010. The global range of subduction zone thermal models. Phys. Earth Planet. Inter. 183, 73–90. https://doi.org/10.1016/j.pepi.2010.02.004

Tiepolo, M., Tribuzio, R., 2005. Slab-melting during Alpine orogeny: Evidence from mafic cumulates of the Adamello batholith (Central Alps, Italy). Chem. Geol. 216, 271–288. https://doi.org/10.1016/j.chemgeo.2004.11.014

Tiepolo, M., Tribuzio, R., Ji, W.Q., Wu, F.Y., Lustrino, M., 2014. Alpine Tethys closure as revealed by amphibole-rich mafic and ultramafic rocks from the Adamello and the Bergell intrusions (Central Alps). J. Geol. Soc. London. 171, 793–799. https://doi.org/10.1144/jgs2013-139

Tiepolo, M., Tribuzio, R., Langone, A., 2011. High-mg andesite petrogenesis by amphibole crystallization and ultramafic crust assimilation: Evidence from Adamello hornblendites (Central Alps, Italy). J. Petrol. 52, 1011–1045. https://doi.org/10.1093/petrology/egr016

Ulmer, P., Callegari, E., Sonderegger, U.C., 1983. Genesis of the mafic and ultramafic rocks and their genetical relations to the tonalitic-trondhjemitic granitoids of the southern part of the Adamello Batholith (Northern Italy). Mem. Soc. Geol. It. 26, 171–222.

Veizer, J., Mackenzie, F.T., 2003. Evolution of sedimentary rocks.

Vermesch, P., 2018. IsoplotR: a free and open toolbox for geochronology. Geoscience Frontiers 9, 1479-1493. https:// doi: 10.1016/j.gsf.2018.04.001.

Vervoort, J.D., Plank, T., Prytulak, J., 2011. The Hf-Nd isotopic composition of marine sediments. Geochim. Cosmochim. Acta 75, 5903–5926. https://doi.org/10.1016/j.gca.2011.07.046

Vervoort, J.D., Kemp, A.I.S., 2016. Clarifying the zircon Hf isotope record of crust-mantle evolution. Chem. Geol. 425, 65–75. https://doi.org/10.1016/j.chemgeo.2016.01.023

Visonà, D., Caironi, V., Carraro, A., Dallai, L., Fioretti, A.M., Fanning, M., 2007. Zircon megacrysts from basalts of the Venetian Volcanic Province (NE Italy): U-Pb ages, oxygen isotopes and REE data. Lithos 94, 168–180. https://doi.org/10.1016/j.lithos.2006.06.007

Wiedenbeck, M., Hanchar, J.M., Peck, W.H., Sylvester, P., Valley, J., Whitehouse, M., Kronz, A., Morishita, Y., Nasdala, L., 2004. Further Characterisation of the 91500 Zircon Crystal 28, 9–39.

Woodhead, J.D., Hergt, J.M., 2005. A preliminary appraisal of seven natural zircon reference materials for in situ Hf isotope determination. Geostand. Geoanalytical Res. 29, 183–195. https://doi.org/10.1111/j.1751-908x.2005.tb00891.x

Zaccaria, D., Vicentini, N., Perna, M.G., Rosatelli, G., Sharygin, V. V., Humphreys-Williams, E., Brownscombe, W., Stoppa, F., 2021. Lamprophyre as the source of zircon in the Veneto region, Italy. Minerals 11, 1–28. https://doi.org/10.3390/min11101081

Figure 1 Click here to access/download;Figure;Fig.1.tif

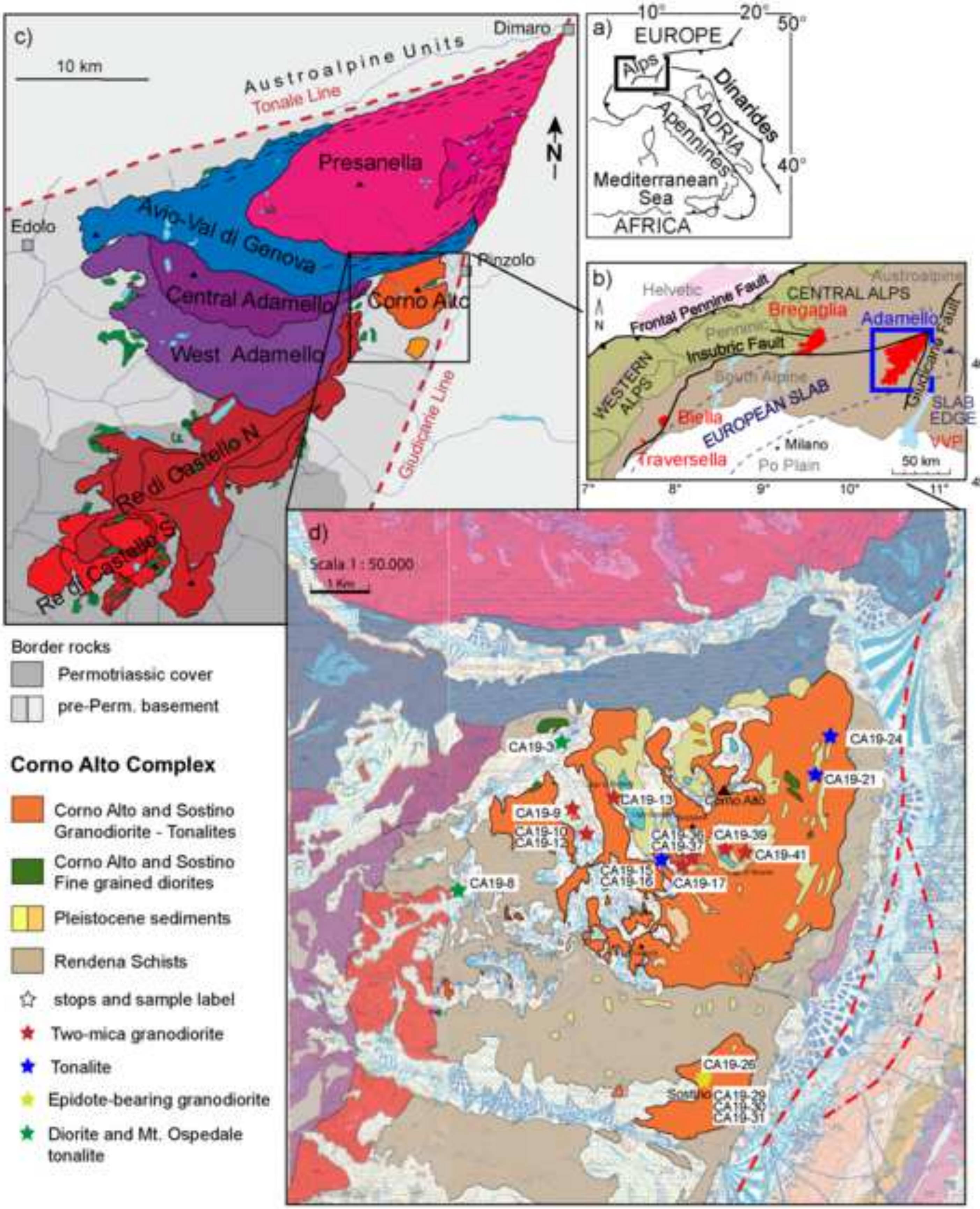

Figure 2

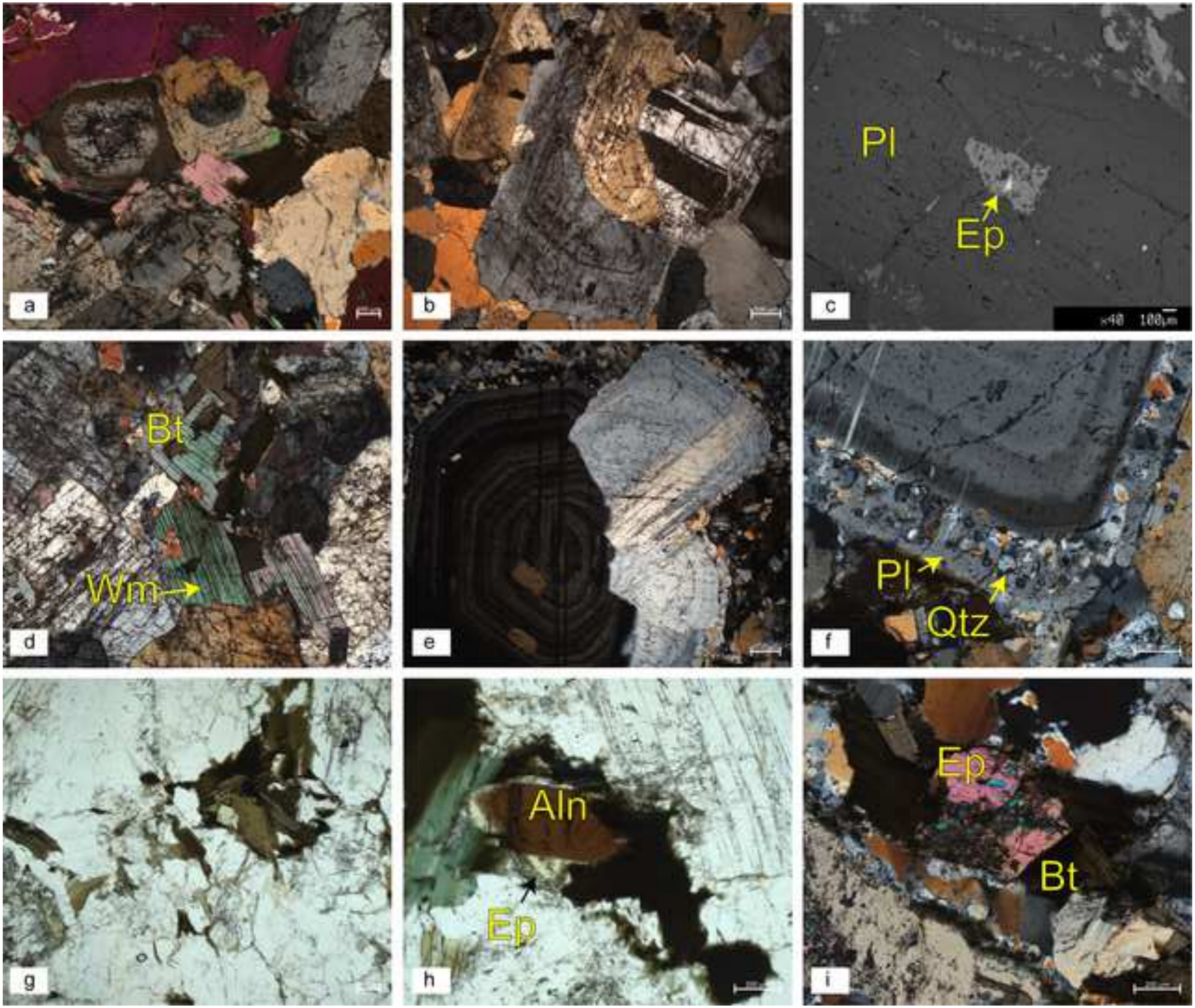

Figure 3

Click here to access/download;Figure;Fig.3.tif

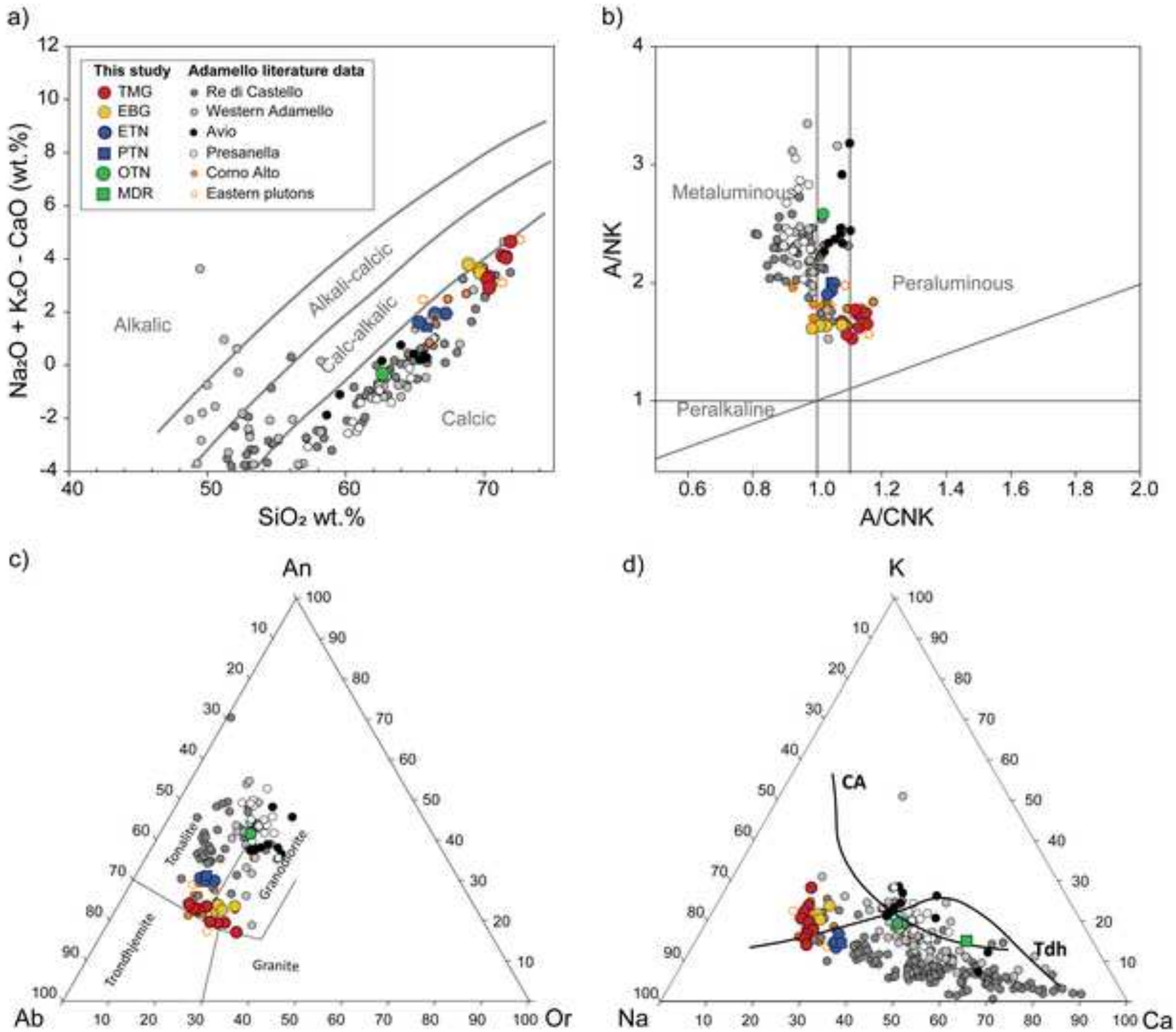

Figure 4

Click here to access/download;Figure;Fig.4.tif

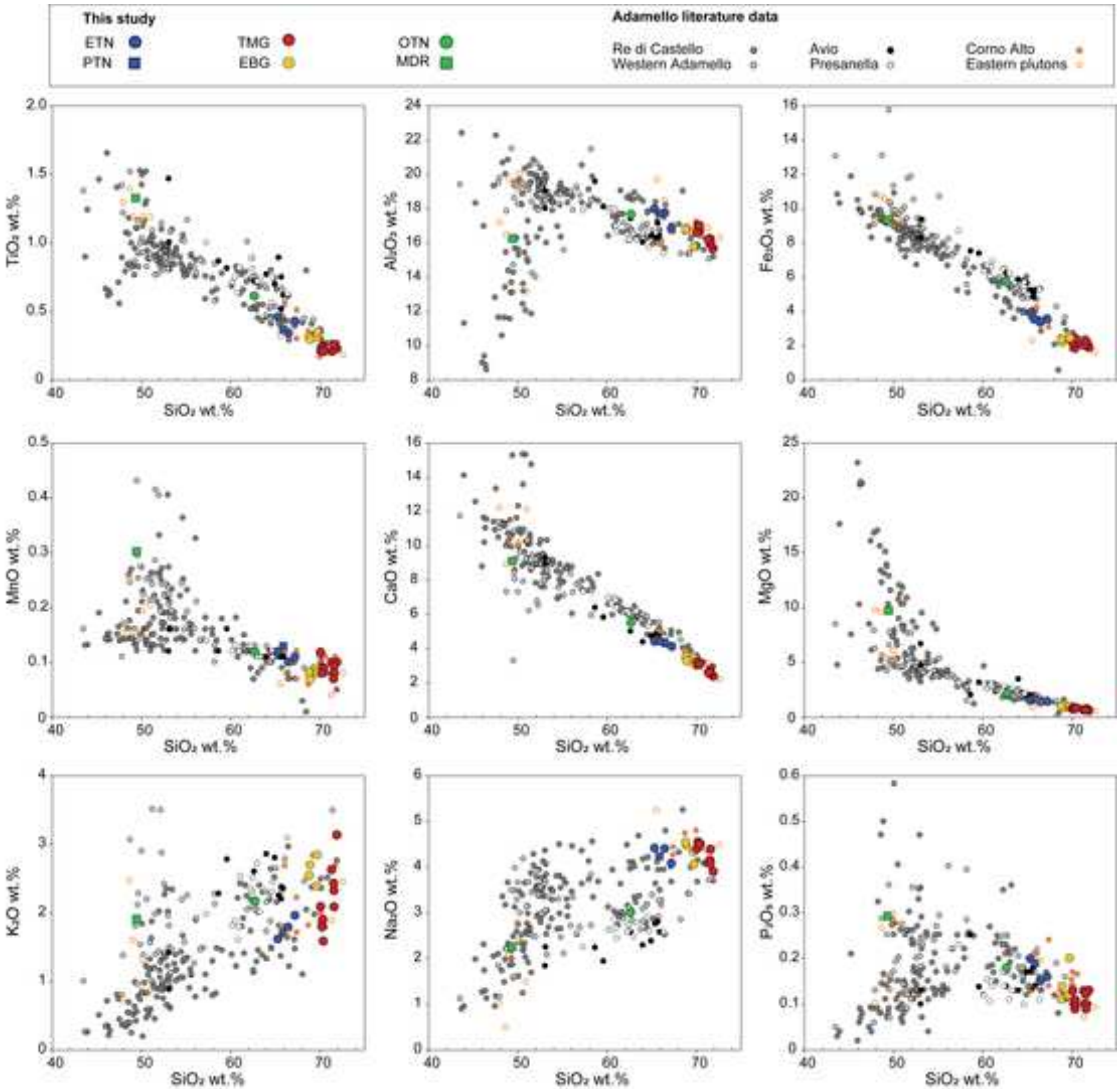

Figure 5

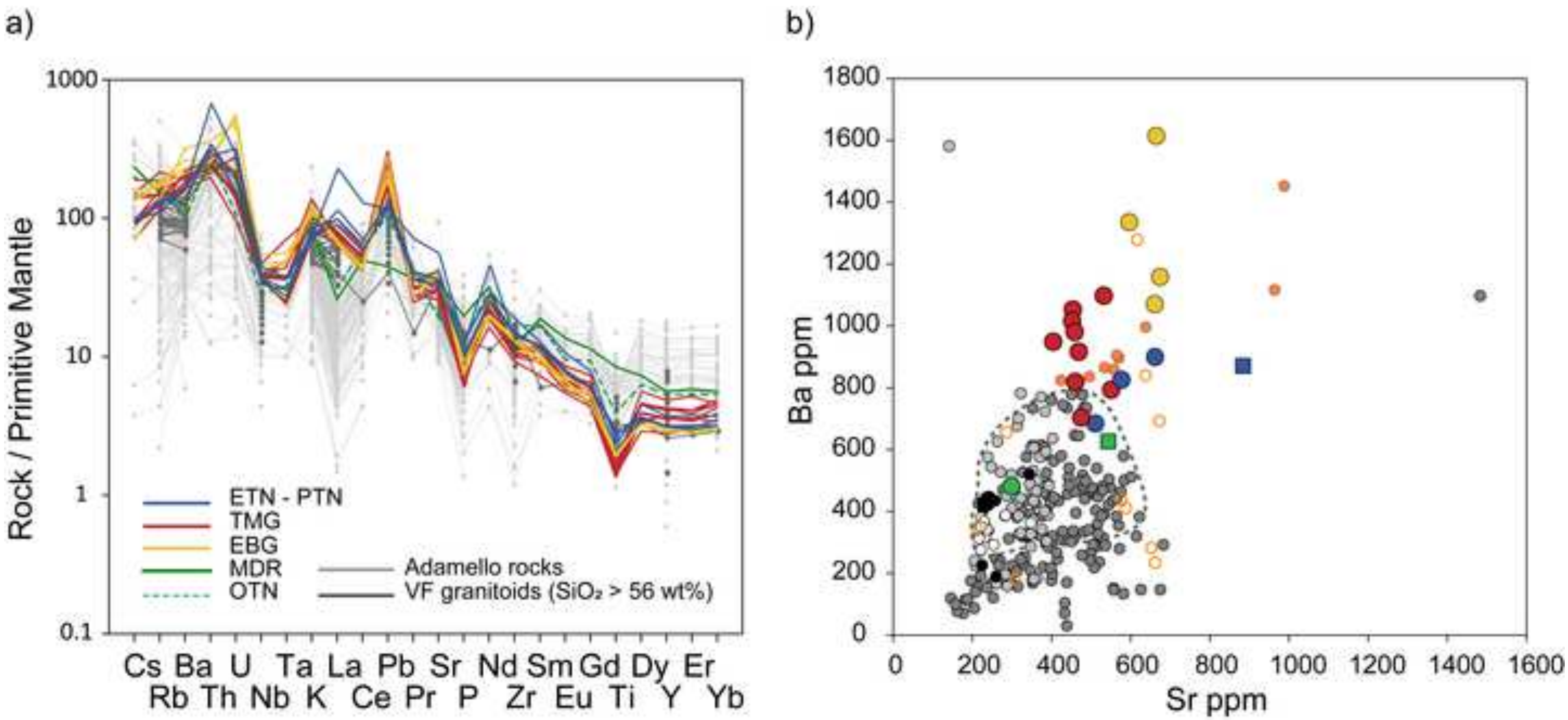
a)
b)
Rock / Primitive Mantle
1000
100
10
1
0.1
Cs Ba U Ta La Pb Sr Nd Sm Gd Dy Er
Rb Th Nb K Ce Pr P Zr Eu Ti Y Yb
ETN - PTN
TMG
EBG
MDR
OTN
Adamello rocks
VF granitoids (SiO₂ > 56 wt%)
Ba ppm
Sr ppm
0
200
400
600
800
1000
1200
1400
1600
1800

Figure 6

Click here to access/download;Figure;Fig.6.tif

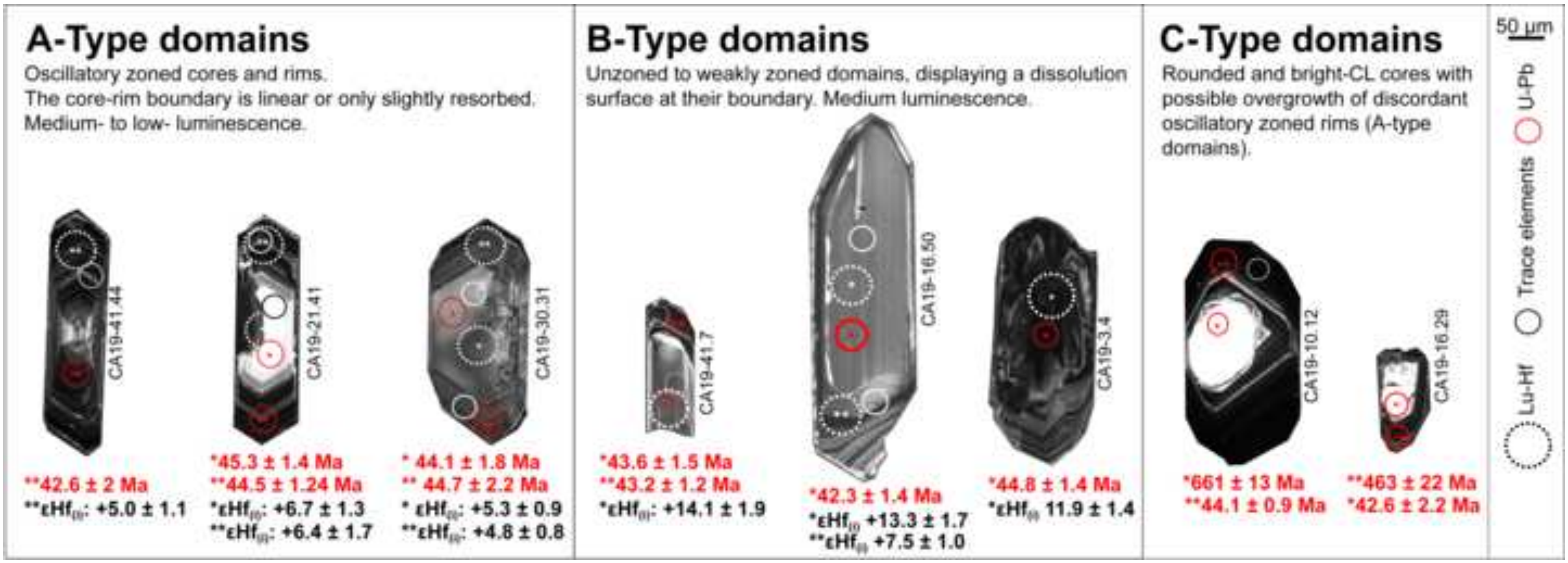

Figure 7

Click here to access/download;Figure;Fig.7.tif

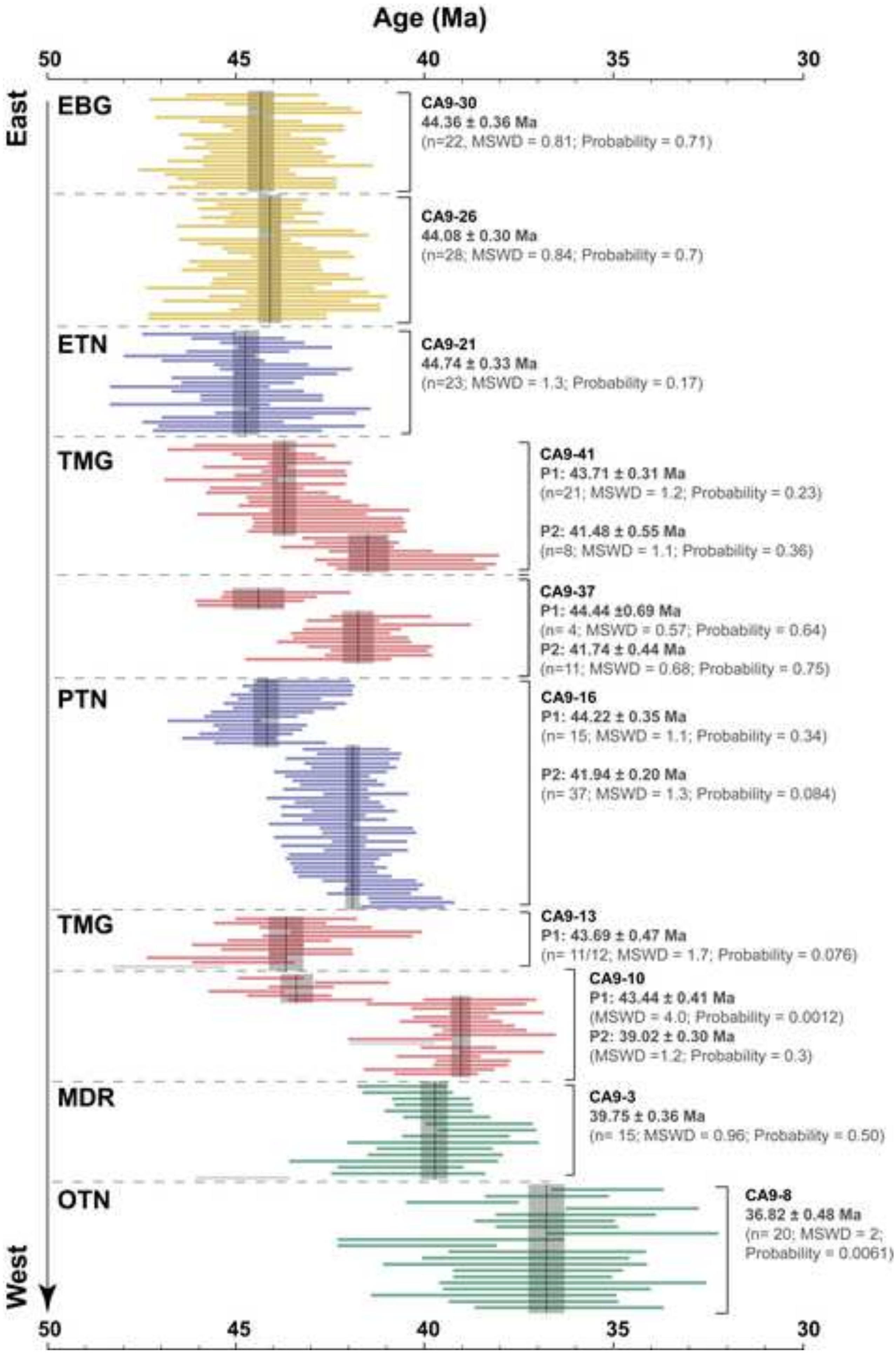

Figure 8

Click here to access/download;Figure;Fig.8.tif

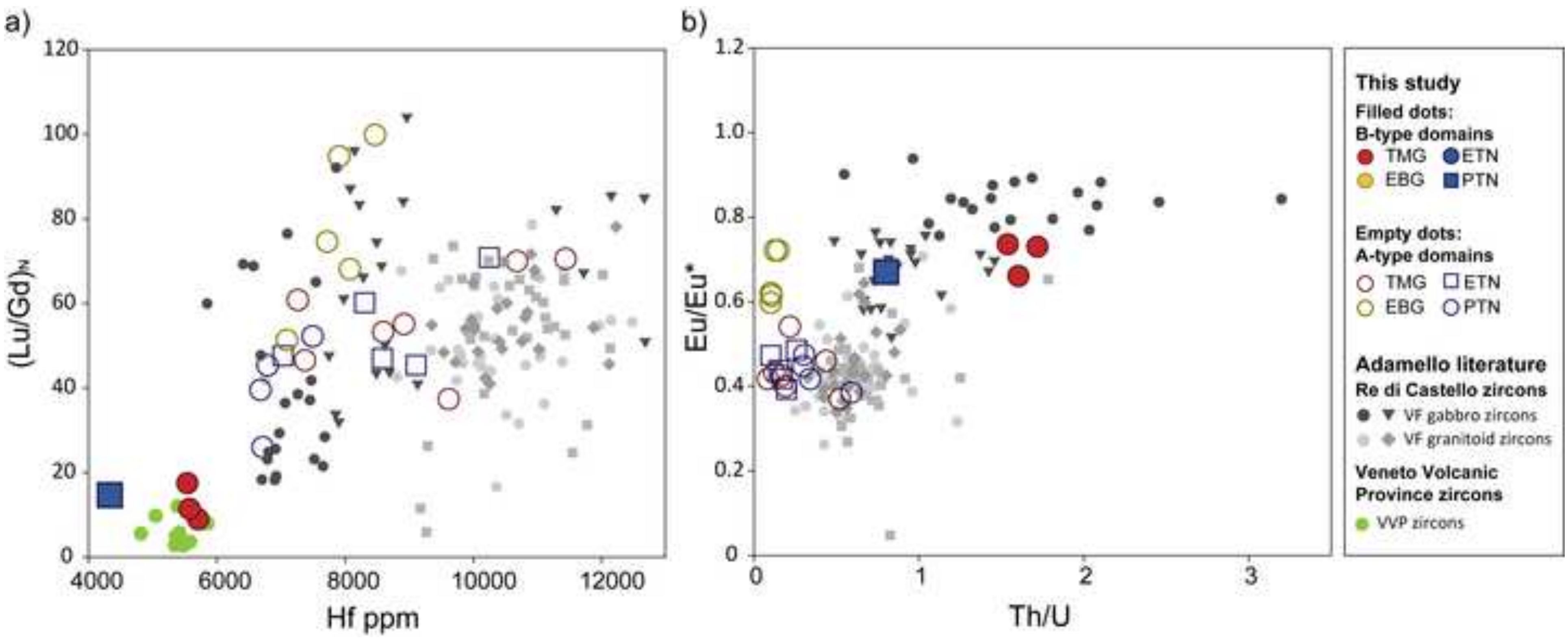

Figure 9

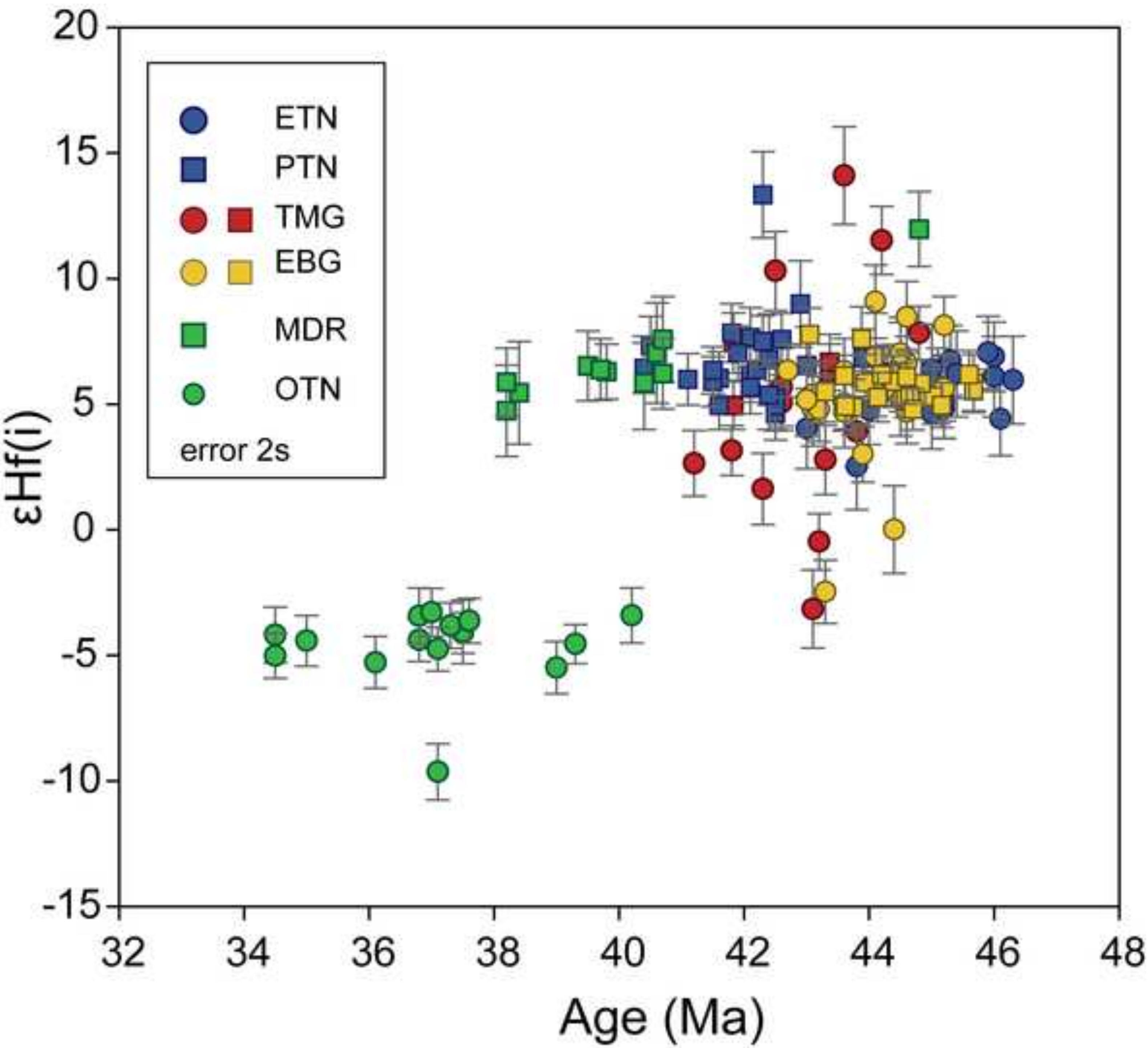

ETN
PTN
TMG
EBG
MDR
OTN
error 2s
εHf(i)
20
15
10
5
0
-5
-10
-15
32
34
36
38
40
42
44
46
48
Age (Ma)

Figure 10

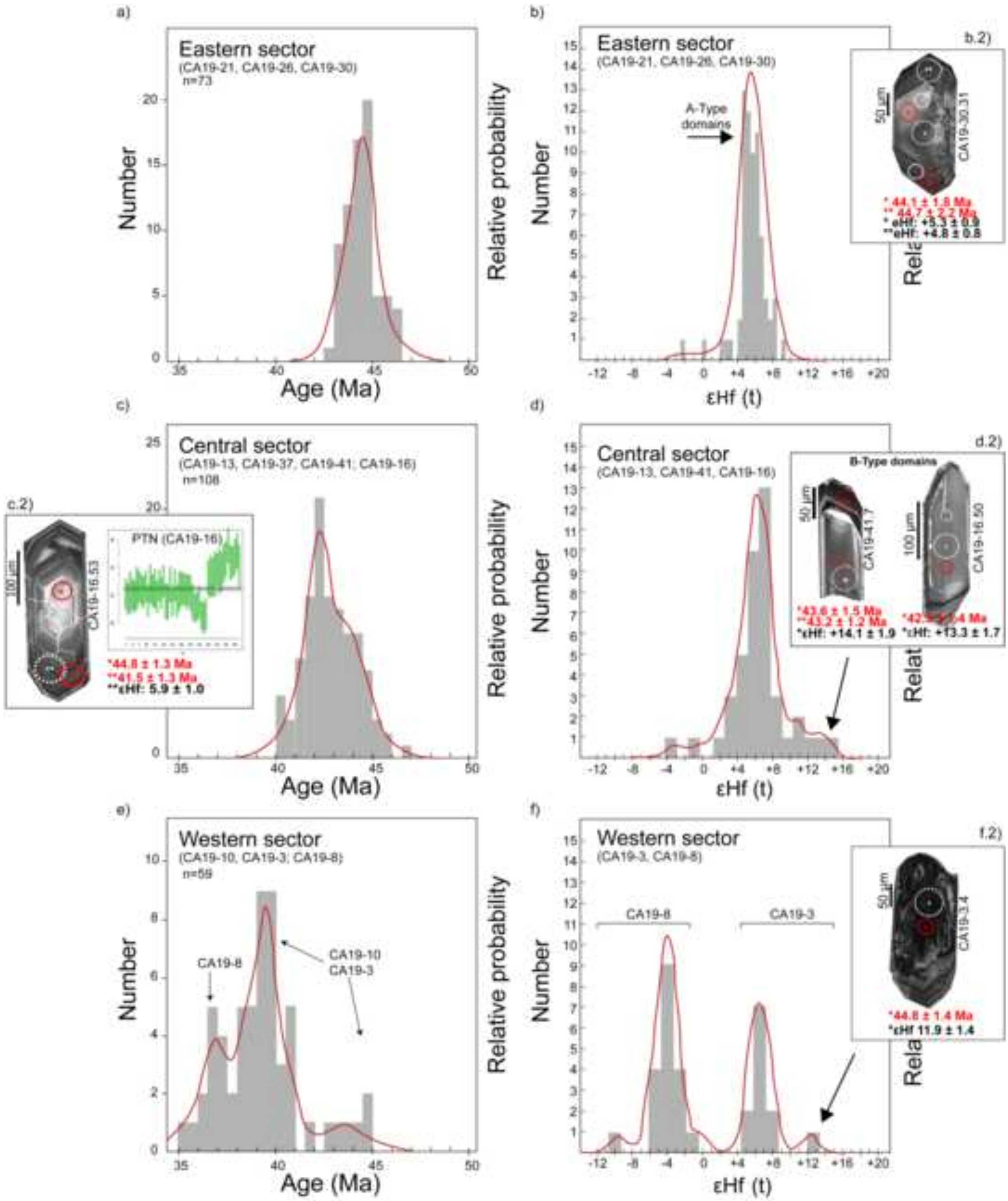
a)
Eastern sector
(CA19-21, CA19-26, CA19-30)
n=73
Number
Age (Ma)
Relative probability
b)
Eastern sector
(CA19-21, CA19-26, CA19-30)
A-Type domains
Number
εHf (t)
b.2)
50 µm
CA19-30.31
*44.1 ± 1.8 Ma
**44.7 ± 2.2 Ma
* εHf: +5.3 ± 0.9
**εHf: +4.8 ± 0.8
c)
Central sector
(CA19-13, CA19-37, CA19-41; CA19-16)
n=108
c.2)
100 µm
CA19-16.53
PTN (CA19-16)
*44.8 ± 1.3 Ma
**41.5 ± 1.3 Ma
**εHf: 5.9 ± 1.0
Age (Ma)
Relative probability
d)
Central sector
(CA19-13, CA19-41, CA19-16)
d.2)
B-Type domains
50 µm
CA19-41.7
100 µm
CA19-16.50
*43.6 ± 1.5 Ma
**43.2 ± 1.2 Ma
*εHf: +14.1 ± 1.9
*εHf: +13.3 ± 1.7
Number
εHf (t)
e)
Western sector
(CA19-10, CA19-3; CA19-8)
n=59
CA19-8
CA19-10
CA19-3
Number
Age (Ma)
Relative probability
f)
Western sector
(CA19-3, CA19-8)
CA19-8
CA19-3
f.2)
50 µm
CA19-3.4
*44.8 ± 1.4 Ma
*εHf 11.9 ± 1.4
Number
εHf (t)

Figure 11

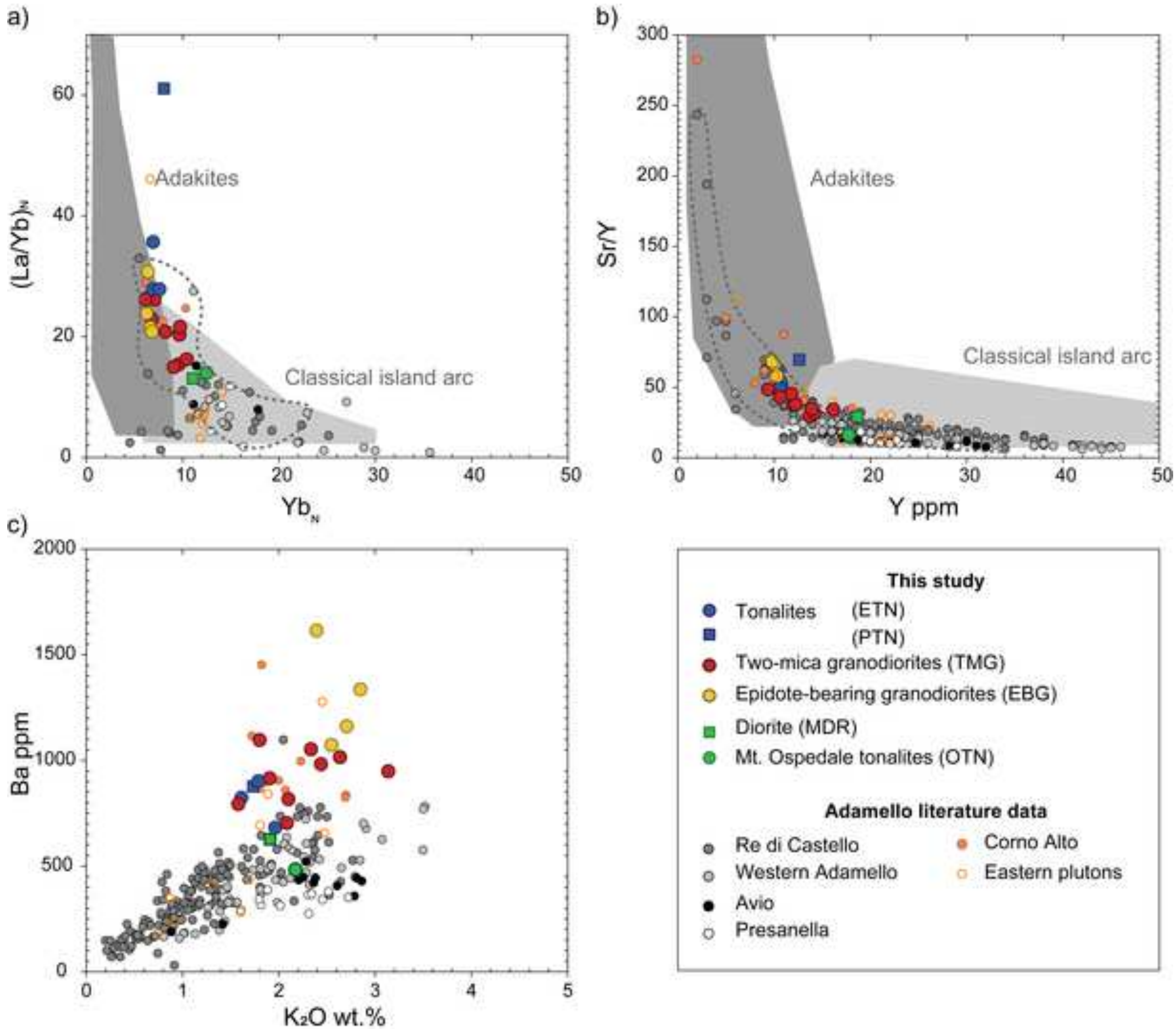

a)
(La/Yb)N
YbN
Adakites
Classical island arc
b)
Sr/Y
Y ppm
Adakites
Classical island arc
c)
Ba ppm
K2O wt.%
This study
Tonalites (ETN)
(PTN)
Two-mica granodiorites (TMG)
Epidote-bearing granodiorites (EBG)
Diorite (MDR)
Mt. Ospedale tonalites (OTN)
Adamello literature data
Re di Castello
Western Adamello
Avio
Presanella
Corno Alto
Eastern plutons

Figure 12

Click here to access/download;Figure;Fig.12.tif

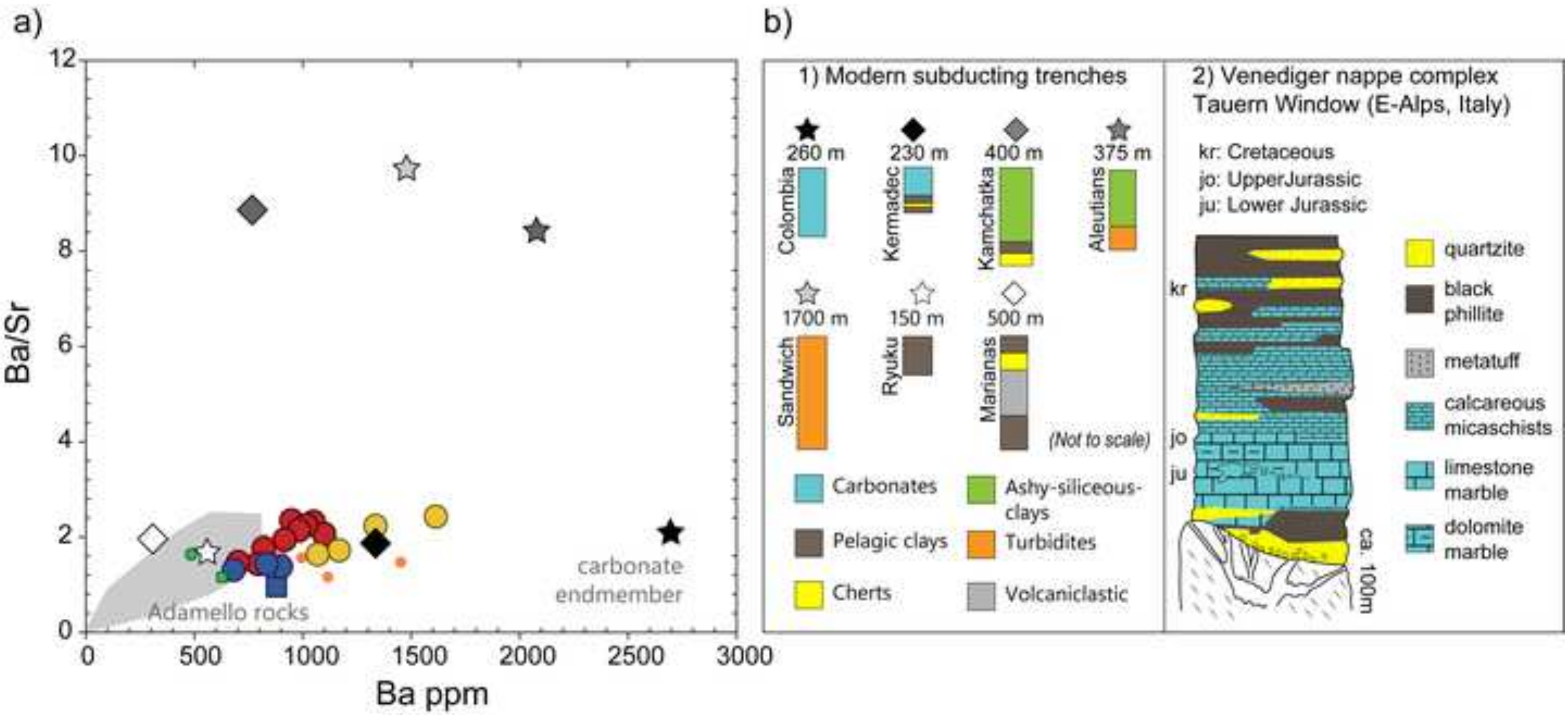

Figure 13

Click here to access/download;Figure;Fig.13.tif

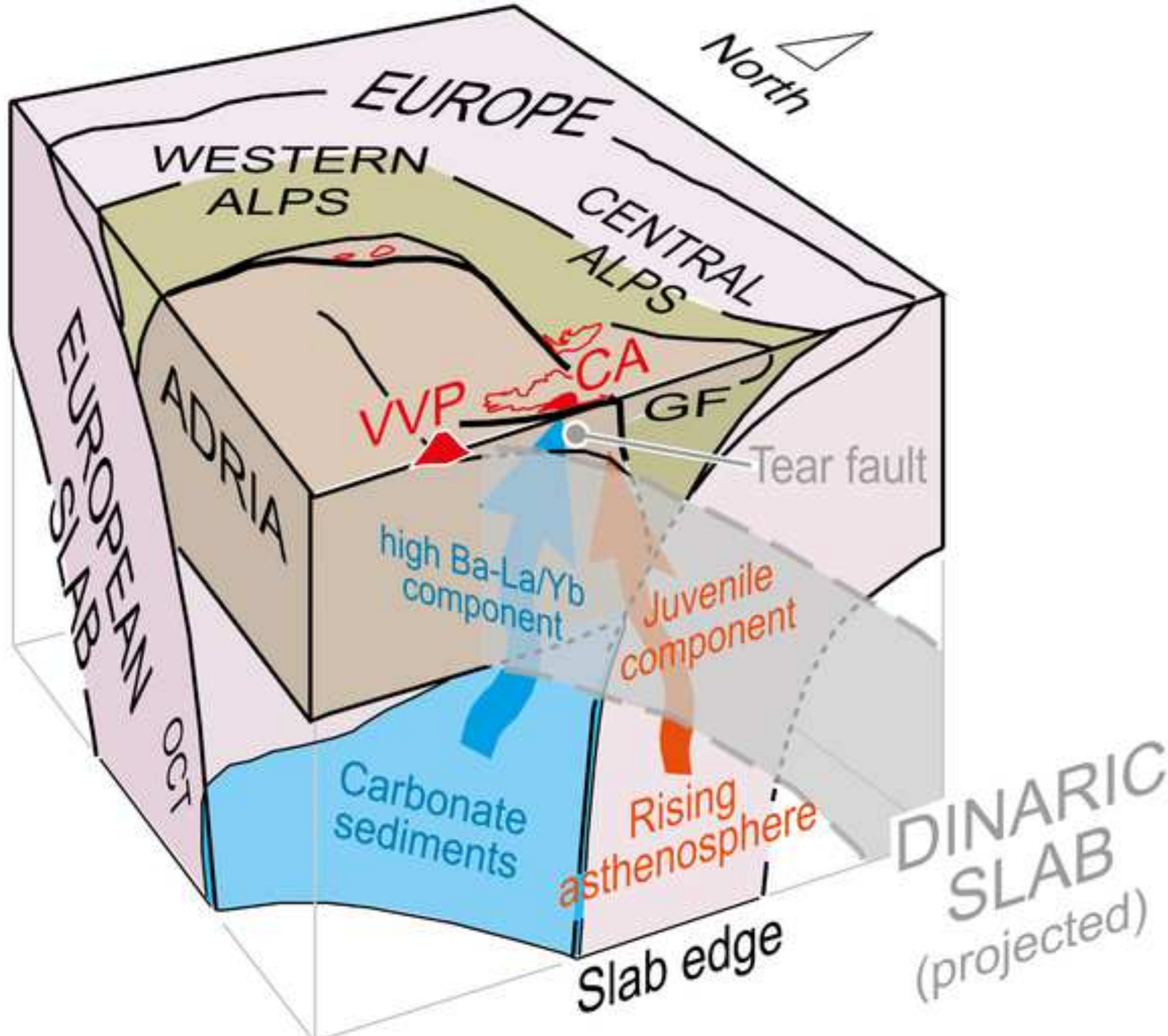

Supplementary material B (Tables)

Click here to access/download

Supplementary material/Appendix (Files for online publication only)

B_MineralChemistry.xlsx

Supplementary material C (Tables)

Click here to access/download

Supplementary material/Appendix (Files for online publication only)

C_ZirconGeochemistry.xlsx